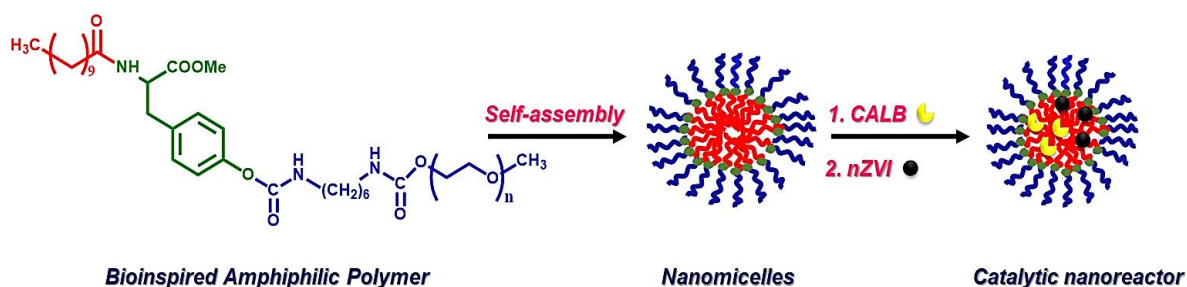# Chapter 5

Candida antarctica Lipase B and nZVI co-loaded bioinspired nanomicelles: A sustainable catalytic nanoreactor for cascade synthesis of p-aminophenol

Bioinspired Amphiphilic Polymer — Self-assembly → Nanomicelles — 1. CALB 2. nZVI → Catalytic nanoreactor

- Eco-compatible nanoreactor
- One Pot Chemoenzymatic Cascade synthesis
- Mild reaction conditions
- Aquoues reaction medium
- Recyclable

NaBH$_4$ 35°C
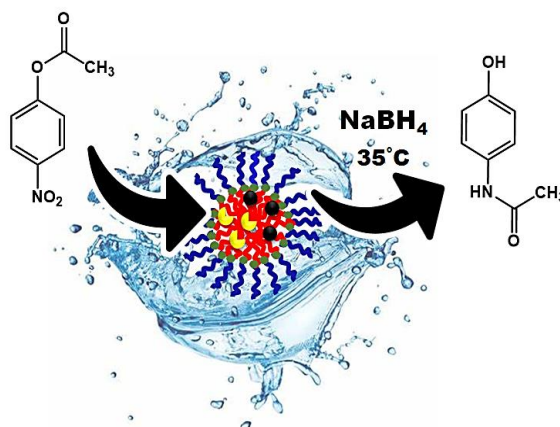
5.1 Introduction

Biocatalysis is an efficient tool to achieve a high degree of regioselectivity, stereoselectivity, and chemoselectivity in challenging organic reactions. Enzymes (catalytic proteins) are biocatalysts and their relevance in nature consists of various chemical processes[1].

Despite being an excellent and potential catalyst, enzymes are sensitive molecules and denaturation can occur if they go beyond their natural environment. Some bottleneck issues are associated with enzymes such as chemical degradation, physical unfolding, and aggregation caused by temperature, pH variations, organic solvents, etc. Enzymes can occasionally get denatured and the reaction sites get distorted and blocked at the end of a single reaction cycle. These issues can be addressed by enzyme immobilization on a suitable support. The main purpose of enzyme immobilization is to enhance the recovery and recycling of the enzyme. An immobilized enzyme depicts superior stability, reusability, control, activity, and tolerance to chemicals or inhibitors compared to a free enzyme[2].

In particular, the most often commercially used enzyme for biocatalysis is lipase (triacylglycerol ester hydrolases, EC 3.1.1.3) due to its broad specificity. Additionally, lipase can be typically used in aqueous media, organic solvents, ionic liquids, supercritical fluids, or deep eutectic solvents without losing its stability but lacks recyclability. Thus, the implementation of immobilized lipase in organic transformations has wide range of potential use in industrial applications. *Candida antarctica* lipase B (CALB) is one of the most stable lipases that has been commercialized, and its immobilized products have numerous applications in organic synthesis[2].

Various materials have been employed as a support for the immobilization of enzymes. These consist of synthetic polymers (polystyrene, polyacrylonitrile (PAN), etc.)[3],[4], inorganic materials (silica, graphene oxide, etc.)[5],[6],[7], natural polymers (chitosan, cellulose, etc.)[8],[9], surfactants (triton x-600)[10].

Enzymes play a critical role in stabilizing the metal nanoparticles, *in situ* formation of nanoparticles, controlling the size of nanoparticles, and acting as a protein framework[11]. The metal nanoparticles are well dispersed in the protein network without agglomeration. Hence, the use of enzymes with nanoparticles introduces a novel idea of nanohybrid materials in which synthesized biohybrids combine a three-dimensional environment with high selectivity (provided by the enzyme) and a broad range of catalysis (provided by the synthesized metal nanoparticles). This

represents an exceptional opportunity to produce materials with multiple catalytic activities. Multistep catalytic reactions can be performed simply via co-immobilization of enzymes, with the utilization of advanced materials as supports, especially nanoscale materials.

Literature reports indicate that highly dispersed ultra-small precious metal nanoparticles (Ag, Au, Pd or Pt) are generated in situ and embedded on the CALB protein structure in aqueous media and at room temperature[11]. Compared to noble metals low-cost metal such as iron offer a cost-effective alternative for commercial appilcations[12]. For instance, Palomo and coworkers reported the synthesis of ultrathin CALB protein iron (II) carbonate nanorods heterogenous bionanohybrid for oxidation, reduction and C-C coupling reaction[13]. Zerovalent iron nanoparticles (nZVI) are known to possess excellent magnetic response and a facile synthesis process, large specific surface area, reusability and separability[14]. nZVI has been exploited as support for enzyme immobilization via direct physical adsorption or immobilization after post-modification. However they have a tendency to agglomerate which can result in low immobilization of enzymes and a decrease in their activity[15].

To address the abovementioned challenges, we report for the first time a facile strategy by rational design of nanoreactors from amino acid derived polymer micelles which can house both enzyme and iron nanoparticle effectively and results in efficient cascade catalysis. The amphiphilic polymers are derived from biocompatible precursors such as tyrosine, polyethylene glycol and undecanoic acid that consequently self-assembled to nanomicelles. Such biomolecules derived sustainable amphiphilic polymers micelles and vesicles have gained a lot of attention in the recent past[16] However they are mostly employed for biomedical applications and not for catalysis. We have directed our efforts to stabilize both *Candida antarctica* lipase B (enzyme)and nZVI (metal nanoparticles) in nanomicelles, to obtain catalytic nanoreactors for one pot chemoenzymatic catalysis. CALB has been used as a model enzyme due to its wide application in industrial biocatalysis. The nanomicelles are termed as nanoreactors, as they are coloaded with both, enzyme and metal in the hydrophobic core. The catalytic efficiency of the tyrosine derived nanoreactors was investigated for hydrolysis of a series of p-nitrophenyl esters and the conditions were optimized. The catalytic activity results from the formation of a substrate-catalyst complex through hydrophobic interaction[17]. Moreover, the cascade synthesis of p-acetaminophen from p-nitrophenylacetate was achieved in a single pot without the need of acid catalyst and organic solvent. This cascade approach leads to reduction of solvents and waste generated (byproduct)

obtained during product isolation, high atom economy, and reduction of workup procedures by diminishing the number of synthetic steps[18]. To the best of our knowledge, this is the first report on synthesis of amino acid derived nanobiohybrid catalyst loaded with *Candida antarctica* Lipase B and nZVI that act as nanoreactors for the synthesis of p-acetaminophen at mild reaction conditions.

5.2 Experimental Section

5.2.1 Materials

Boc-L-tyrosine methyl ester (99.0%), Poly(ethylene glycol)methyl ether, (mPEG, Mn = 5.0 kg/mol), hexamethylene diisocyanate (HMDI), undecanoic acid (99%), trifluoroacetic acid (TFA), 1,4-diazabicyclo [2.2.2] octane (DABCO), phosphate buffer saline tablets (for preparation of pH 7.4 buffer solution), *Candida antarctica* Lipase B (CALB), p-nitrophenyl acetate, p-nitrophenyl butyrate, p-nitrophenyl palmitate, p-nitrophenyl octanoate, p-nitrophenyl decanoate and p-nitrophenyl chloroformate were purchased from Sigma Aldrich, Mumbai, India. Various solvents (acetonitrile, N, N-dimethylformamide (DMF), dimethyl sulfoxide (DMSO), acetone and dichloromethane (DCM)) were obtained from Sisco Research Laboratories, Mumbai, India. Other reagents were of analytical grade, purchased from commercial sources, and used as received without further purification. The solutions were prepared using de-ionized water.

.

5.2.2 Characterization

Nuclear Magnetic Resonance: Nuclear magnetic resonance (^{1}H NMR) spectra were recorded on a Bruker Avance 500 MHz spectrometer using DMSO-d_6 as solvent and tetramethyl silane as an internal standard.

Fourier Transform Infrared Spectroscopy (FTIR): Fourier transform infrared spectroscopy measurements were performed on a Bruker Alpha IR spectrophotometer. The samples were ground with KBr and turned into pellets by disc pressing. The spectra were recorded in the 400-4000 cm^{-1} range.

Thermogravimetric analysis (TGA): Using a TGA 2950 instrument, thermogravimetric analysis of the polymer was carried out in the temperature range of 25 to 750 °C under flowing N$_2$ (30 mL min^{-1}) with a heating rate of 10 °C min^{-1}.

High-resolution transmission microscopy (HR-TEM). For high-resolution transmission microscopy (HR-TEM), the samples were diluted and were dispersed on carbon-coated copper grids. The sample-coated copper grids were then air-dried overnight at ambient temperature. The images of the samples were then recorded on a Jeol (Jem-2100F) electron microscope at an accelerating voltage of 200 kV.

Field Emission Gun Scanning Electron Microscopy (FEG-SEM). A JSM-7600 F field emission scanning electron microscope was employed to characterize the morphology. The samples for SEM characterization were treated by spraying a thin platinum layer on their surface under vacuum conditions to enhance their conductivity.

Dynamic Light Scattering (DLS): Dynamic light scattering (DLS) was used to determine the hydrodynamic diameter and polydispersity of micelles in the solution which was performed on Beckman Coulter Delso Nano.

Atomic Force Microscopy: AFM images were recorded on NTEGRA PRIMA, NT-MDT, Russia.

Inductively coupled plasma atomic emission spectroscopy (ICP-AES). The palladium concentration in the catalyst was measured with a Simultaneous ICP Spectrometer, ARCOS, SPECTRO Analytical GmbH, Germany.

UV-visible spectrophotometry: UV-vis spectrophotometric determinations were done using a Perkin Elmer Lambda 35.

Florescence spectroscopy: Fluorescence spectra were scanned on a JASCO FP-6300.

Vibrating sample magnetometer (VSM): Vibrating sample magnetometer (VSM) analysis was performed using a VSM 7410, Lakeshore, Sweden at room temperature.

Circular Dichroism spectroscopy: CD analysis was performed on a J 815(JASCO) spectrometer to investigate the free enzyme and catalyst.

5.2.3 Synthesis of Tyrosine derived amphiphilic polymers.

The general strategy for the synthesis of tyrosine-derived amphiphilic polymer involves the introduction of a hydrophilic mPEG segment and hydrophobic alkyl side chain to introduce an appropriate amphiphilicity in the polymer structure and to achieve the self-assembly of amphiphilic polymer to nanomicelles in an aqueous medium.

5.2.3.1 PEGylation of Boc protected Tyrosine (Boc-Tyrosine-mPEG) (Step 1):

To a solution of Boc-L-tyrosine methyl ester (0.500 g, 1.6 mmol) and mPEG (0.2 g, 0.004 mmol) in DMF (10 mL), HMDI (200 μL,) was added. DABCO (5.0 mg) was added as a catalyst, and the reaction was proceeded at 60 °C for 3 h. The insoluble white product formed was separated from the reaction mixture by filteration. The filtrate obtained was reprecipitated in water to obtain a white solid and separated by vacuum filtration followed by washing with acetone and diethyl ether. The resulting solid was dissolved in 10 mL DMSO and further purified by dialyzing the polymer solution using a dialysis membrane (MWCO 3500 Da) against water to remove the low molecular weight polymers. The purified polymer solution was lyophilized to obtain a white polymer and stored under a vacuum until further use. The yield was 70%.

^{1}H NMR (500 MHz, DMSO-d$_6$): δ 8.5 (1H, NH amide of Boc), 7.6 (1H, −NH of urethane), 7.3-6.6 (4H, −CH aromatic protons of tyrosine), 5.7 (2H, -CH$_2$ directly attached to -NH of urethane), 4.15-4.06 (1H, CH proton of tyrosine), 3.7 (3H, -CH$_3$ proton of methyl ester), 3.61 (2H, −CH$_2$ protons of tyrosine), 3.51-3.02 (−OCH$_2$, -OCH$_3$ characteristic peak of mPEG), 2.9-1.33 (−CH$_2$ protons of HMDI) and 1.45 (-CH$_3$ protons of Boc).

FTIR (KBR pellet, wavenumber (cm^{-1})): 3336 (N-H stretch), 2933, 2858(C−H stretch aromatic) 1740 (C=O of methyl ester), 1686 (C=O of urethane), 1626 (C=O of Boc),1572 (C-N of amide), 1230 (C−O of ester).

5.2.3.2 Deprotection of Boc-Tyrosine-mPEG (Step 2):

PEGylated Boc-L-Tyrosine-methyl ester (0.5 g) was dissolved in 5 mL of dried DMSO to which 4 mL of TFA was added and stirred for 1h at 0-5 °C. Then the reaction was allowed to be stirred at room temperature (35 °C) for 1 h. TFA was removed from the reaction mixture using a rota-evaporator, the polymer was further purified by dialyzing against water using a dialysis membrane (MWCO 3500 Da) for 24 h, and then the sample was lyophilized to get yellowish-colored powder. %Yield= 72%

^{1}H NMR (500 MHz, DMSO-d$_6$): 8.5 (1H, -NH of urethane), 7.1-7.4 (−CH aromatic protons of tyrosine), 5.7 (2H, -CH$_2$ directly attached to -NH of urethane), 4.15-4.06 (1H, CH proton of

tyrosine), 3.0 (2H, free amine), 3.61 (2H, −CH$_2$ protons of tyrosine), 3.4-3.5 (1H, −OCH$_2$ characteristic peak of mPEG), 1.2-1.33 (−CH$_2$ protons of HMDI).

FTIR (KBR pellet): wavenumber (cm^{-1}): 3345 (N-H stretch), 2934, 2861(C−H stretch aromatic), 1739 (C=O of ester), 1707 (C=O of urethane), 1216 (C−O of ester).

5.2.3.3 Conjugation of Tyr-mPEG polymer with undecanoic acid via amide bond formation (Step 3):

The product obtained in step 2 was dispersed in DMF; undecanoic acid (100 mg, 0.53 mmol) was added and the reaction mixture was sonicated for 15 mins. EDC.HCl (1-ethyl-3-(3-dimethyl aminopropyl) carbodiimide hydrochloride) (100 mg) and NHS (N-hydroxy succinimide) (10 mg) were added and the reaction was kept overnight at room temperature. The product was filtered to remove the byproducts and reprecipitated in cold water. The product was separated by vacuum filtration and washed with water followed by acetone. The polymer was dialyzed for further purification. The obtained product was dried and weighed. (75% yield).

^{1}H NMR (500 MHz, DMSO-d$_6$): δ (ppm) 8.5 (1H, -NH of urethane), 7.1-7.4 (−CH aromatic protons of tyrosine), 5.7 (2H, -CH$_2$ directly attached to -NH of urethane), 4.15-4.06 (1H, CH proton of tyrosine), 5.1 (1H, -NH of amide), 3.61 (2H, −CH$_2$ protons of tyrosine), 3.4-3.5 (1H, −OCH$_2$ characteristic peak of mPEG), 1.2-1.48 (−CH$_2$ protons of HMDI), 2.77-2.99 (-CH$_2$ proton of undecanoic acid).

FTIR (KBR pellet), wavenumber (cm^{-1}): 3334 (N-H stretch), 2929, 2855 (C−H stretch aromatic) 1740 (-C=O of ester), 1688 (-C=O of urethane), 1623 (-C=O of amide), 1230 (C−O of ester).

5.2.3.4 Self-assembly of amphiphilic polymer into micelles and determination of critical micelle concentration.

The micelles were prepared from the tyrosine-derived amphiphilic polymer by the solvent exchange method. Briefly, 10 mg of the amphiphilic polymer was dissolved in 10 mL of DMSO (1 mg/mL concentration). The solution was stirred at 35°C for 1 h and then dialyzed against water using a dialysis membrane (MWCO 3500 Da). The critical micelle concentration (CMC) was determined by fluorescence spectrophotometry using pyrene as a probe. For the determination of CMC, the

polymer concentration was varied from 1.0×10^{-5} mg/mL to 0.1 mg/mL whereas the concentration of pyrene was fixed at 1.0×10^{-3} M. The fluorescence spectra were then recorded at an excitation wavelength of 330 nm. The emission fluorescence at 373 and 384 nm was monitored. The point of intersection on extrapolating the intensity ratio I_{373}/I_{384} in the high and low concentration regions was designated as the CMC value of the synthesized amphiphilic polymer.

5.2.4 Synthesis of catalytic nanoreactors (nZVI-CALB@NM) for chemoenzymatic reactions

Step 1: Synthesis of CALB-loaded nanomicelles (CALB@NM)

For the synthesis of CALB-loaded micelles, 12.5 mg of CALB was dispersed in PBS buffer and then slowly added to the nanomicellar solution (1mg/mL) dropwise. The resulting solution was allowed to stir for 5 h on magnetic stirrer and then incubated in refrigerator at 4°C for 2 h. The resulting solution was subjected to dialysis against PBS buffer (10 Mm, pH= 7.0). The resulting solution in the dialysis bag was the desired CALB loaded nanomicelles (CALB@NM).

Step 2: Synthesis of zerovalent iron nanoparticle-loaded CALB@NM.

To prepare nZVI-CALB@NM, 10 mL FeCl$_3$ solution (0.3 M) was sonicated for 10 min. Then, 10 mL NaBH$_4$ (0.8 M) solution was added dropwise during the course of 10 min to the FeCl$_3$ solution in an inert condition with nitrogen purging. The reaction mixture was sonicated for the next 30 min, to ensure the complete reduction of Fe^{3+} ions to zero-valent iron (Fe^0) nanoparticles. To this reaction mixture sodium hydroxide was added dropwise to adjust the pH 8. The resultant solution was sonicated for 10 min. The synthesized nanoparticles were separated by magnetic decantation followed by washing with methanol and acetone thrice to remove excess borohydride and byproducts. Next, CALB@NM solution (10mL) was added dropwise and the resultant solution was kept on stirring for 30 mins in an inert condition with nitrogen purging. The reaction mixture was subjected to dialysis against PBS buffer (10 Mm, pH= 7.0). The obtained product was then stored in a refrigerator.

5.2.5 Determination of *Candida antarctica* Lipase B loading in micelle:

The amount of lipase bound in the nanomicelles via hydrophobic interactions was determined by

Bradford assay. Loading of CALB was done by dialysis method. For this purpose, 5 mg of polymer and 12.5 mg of CALB were taken in DMSO (5 mL), Mili-Q water (5 mL) was added to this solution dropwise and stirred for 4 h. The solution was transferred to dialysis bag of MWCO 3500 Da and dialyzed for 24 h against 150 mL of PBS buffer (10 mM, pH 7.0) to remove the unencapsulated enzyme. Fresh PBS was replenished periodically. The dialyzed transparent solution was preserved, and the dialysis media was subjected to Bradford assay to determine the free lipase. All the experiments were carried out in triplicate. The loading of total protein can be calculated from equation (1).

$$\text{Loading (\%)} = \frac{\text{total protein} - \text{protein in dialysis media}}{\text{total protein content}} \times 100$$

5.2.6 Amount of zerovalent iron nanoparticles loading in nZVI-CALB@NM

The amount of incorporated zerovalent iron nanoparticles was determined from the iron content analyzed by Inductively Coupled Plasma Atomic Emission Spectroscopy (ICP-AES), after the acid digestion of sample. For this protocol, 10 mg of polymer and 50 mg of synthesized zerovalent iron nanoparticles were taken in DMSO (5 mL), Mili-Q water (5 mL) was added to this solution dropwise and stirred for 6 hours. The solution was transferred to semi-permeable membrane of MWCO 3500 Da and dialyzed for 24 h against 250 mL of PBS buffer (10 mM, pH 7.0) to remove the unencapsulated iron. Fresh PBS was replenished periodically. The dialyzed transparent solution was preserved, and the dialysis media was utilized for the ICP-AES analysis.

5.2.7 Hydrolytic activity of nZVI-CALB@NM.

The hydrolytic activity of the catalyst was determined using p-nitrophenyl acetate (p-NPA) as a substrate. In an enzyme activity assay, 50 µL of p-NPA (100 mM) was first dissolved in acetonitrile and the 2 mL nZVI-CALB@NM (catalyst) were incubated at 37˚C. The release of p-nitrophenol was then monitored using a UV-vis spectrophotometer (Agilent Cary60) at a wavelength of 405 nm for 30 minutes at room temperature.

5.2.8 Hydrogenation activity of nZVI-CALB@NM.

The catalytic activity of the nZVI-CALB@NM was measured using p-nitrophenol as a substrate.

Briefly, a 2 mL reaction mixture containing catalyst (18 wt% nZVI), 1 mL, 1 mM of p-nitrophenol and 1.4 mM NaBH$_4$ was stirred at room temperature. This mixture was stirred until the reaction was completed. The reaction progress was spectrophotometrically monitored at 405 nm using a UV−vis spectrophotometer for 10 min. Each 50 μL aliquot of the sample was diluted in 450 μL of distilled water. The hydrogenation activity was determined as a pseudo first-order reaction.

5.2.9 Kinetic evaluation of reduction of 4-Nitrophenol

The kinetics of reduction reaction was also determined in terms of concentration of 4-NP. It is assumed that no reaction takes place initially due to a time delay. This time delay is defined as an induction period before the commencement of reaction wherein a restructuring of the nanoparticle surface takes place. The restructuring of surface atoms generates catalytically active sites like corners or edges. This helps the initiation of the reaction. It was noted that the pseudo first order reaction kinetics could be employed for the reduction of 4-NP to 4-AP. As the concentration of NaBH$_4$ is far greater than that of 4-NP, the reaction rate is presumably independent of NaBH$_4$ concentration. Hence the rate of the reaction can be evaluated by studying the kinetics of the reaction in terms of the concentration of 4-NP[19]. The rate constant k was determined for the reaction using the plot of ln (Ct/C$_0$) vs. reduction time as per the following equation (Eq. (2)):

$$\ln\left(\frac{Ct}{Co}\right) = -kt \tag{2}$$

Where Ct is the concentration of the 4-NP at time t (min), C$_0$ is the initial concentration of 4-NP at time t = 0 (min) and k is rate constant. The conversion of 4-NP was calculated using the following equation (Eq. (2)):

$$\text{Conversion} = \ln\left(\frac{At}{Ao}\right) X \ 100\% \tag{3}$$

where At presents the UV absorbance at 405 nm, which is proportional to the concentration of reduced 4-NP; A0 is initial UV absorbance at 405 nm after addition of NaBH$_4$.

5.2.10 Multistep catalytic synthesis of acetaminophen using nZVI-CALB@NM.

The synthesis of acetaminophen was carried out in a one-pot by mixing 10 mM of p-NPA substrate

with nZVI-CALB@NM in a final reaction volume of 2 mL. Subsequently, 50.5 mg of $NaBH_4$ was added to initiate the hydrogenation reaction. To measure the release of p-NP from p-NPA, UV−visible spectra with a wavelength ranging from 250 to 500 nm were scanned. The hydrogenation of 4-nitrophenol to 4-aminophenol was also monitored at 405 nm via UV−visible spectrophotometry for 10 min at 2 min intervals. Finally, 0.1g of acetic acid was added to the reaction mixture. The formation of the final product was monitored at 5 min intervals for next 20 min. All reactions were performed at 35°C with vigorous stirring. For all UV measurements, 50 μL aliquots of the sample were diluted in 450 μL of distilled water.

5.2.11 Recycling studies

To recycle the catalyst, the reaction mixture was filtered. After filtration, the nZVI-CALB@NM catalyst solution separated as a filtrate which was further treated with diethyl ether (3×2 mL) to extract any traces of unreacted substrates. The purified catalyst solution was collected and used for assessment of recycling efficiency for the next cascading cycle.

5.3 Results and Discussion:

5.3.1 Synthesis of Tyrosine-derived amphiphilic polymer

For the synthesis, commercially available Boc-L-tyrosine methyl ester was used as a precursor as shown in **Scheme 5.1**. Tyrosine was chosen as a backbone of the polymer skeleton due to its multifunctionality and inherent biocompatibility. Tyrosine have hydroxyl, amino, and carboxyl functional groups which can be tailored as required. Our synthesis began with the introduction of hydrophilic segment mPEG with a free hydroxyl group via urethane linkage using hexamethylene diisocyanate as a crosslinking agent and resulting in pre-polymer 1. As free amine and carboxyl groups of tyrosine are prone to react with HMDI, hence we chose to work with the Boc-L-tyrosine methyl ester, which only has a free hydroxyl group, protected amine and acid functionalities.
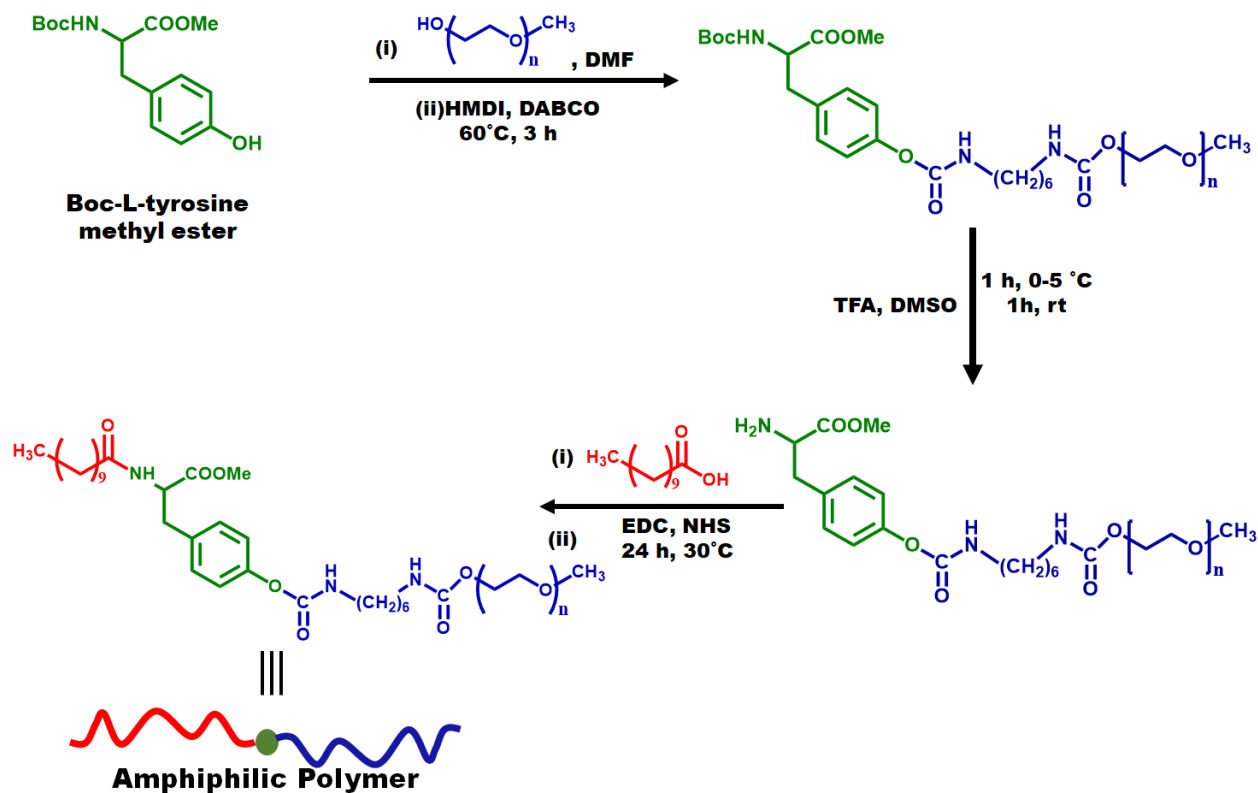
Scheme 5.1: Schematic representation of the synthetic route to Poly (ethylene glycol) methyl ether, M_n=5000 and undecanoic acid-tagged Tyrosine amphiphilic polymer and depicting the self-assembly of tyrosine amphiphilic polymer into nano micelles.

The formation of urethane linkage between Boc-L-tyrosine methyl ester and mPEG was confirmed by the appearance of the characteristic peak of urethane at 7.6 ppm **(Figure 5.1).** The successful conjugation was further supported by FTIR analysis which showed a carbonyl peak of urethane at 1686 cm^{-1} (**Figure S1**). Further, the Boc-protected amine of tyrosine was deprotected using trifluoroacetic acid to obtain pre-polymer 2 with a free amine group for further functionalizations[20].
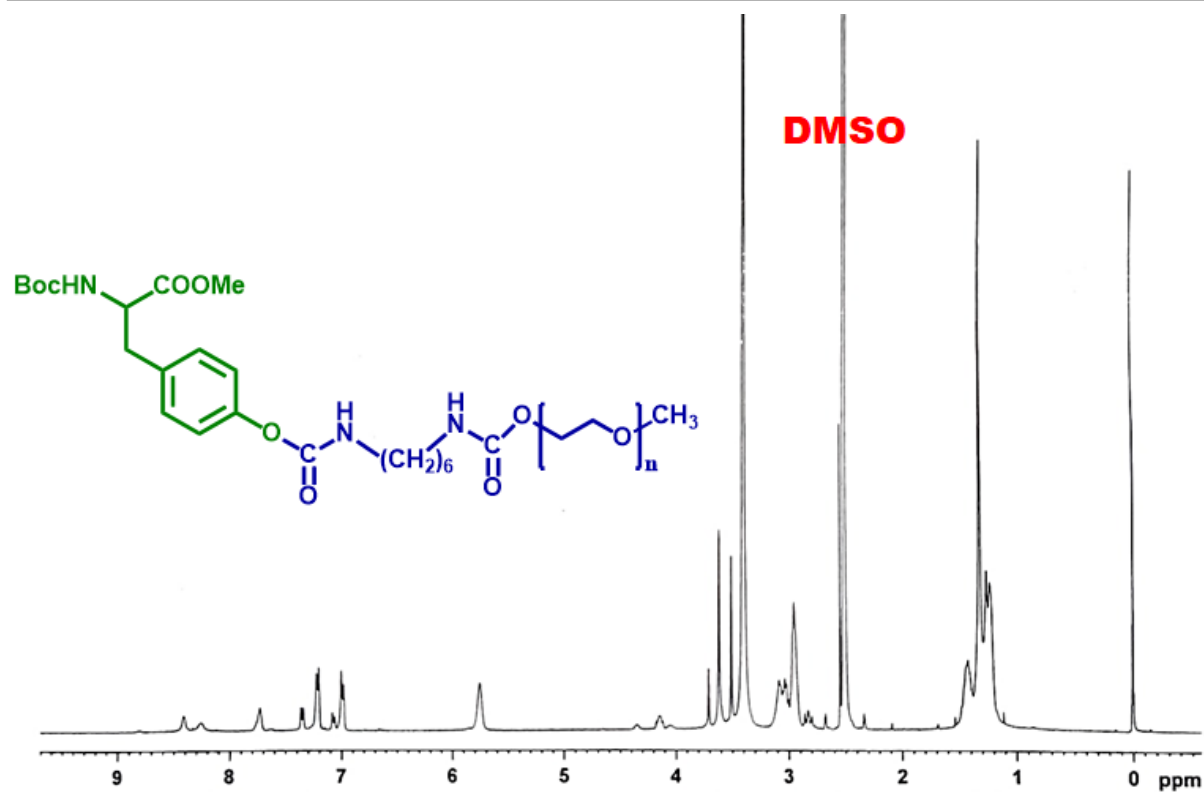
Figure 5.1: ¹H NMR of pre-polymer 1
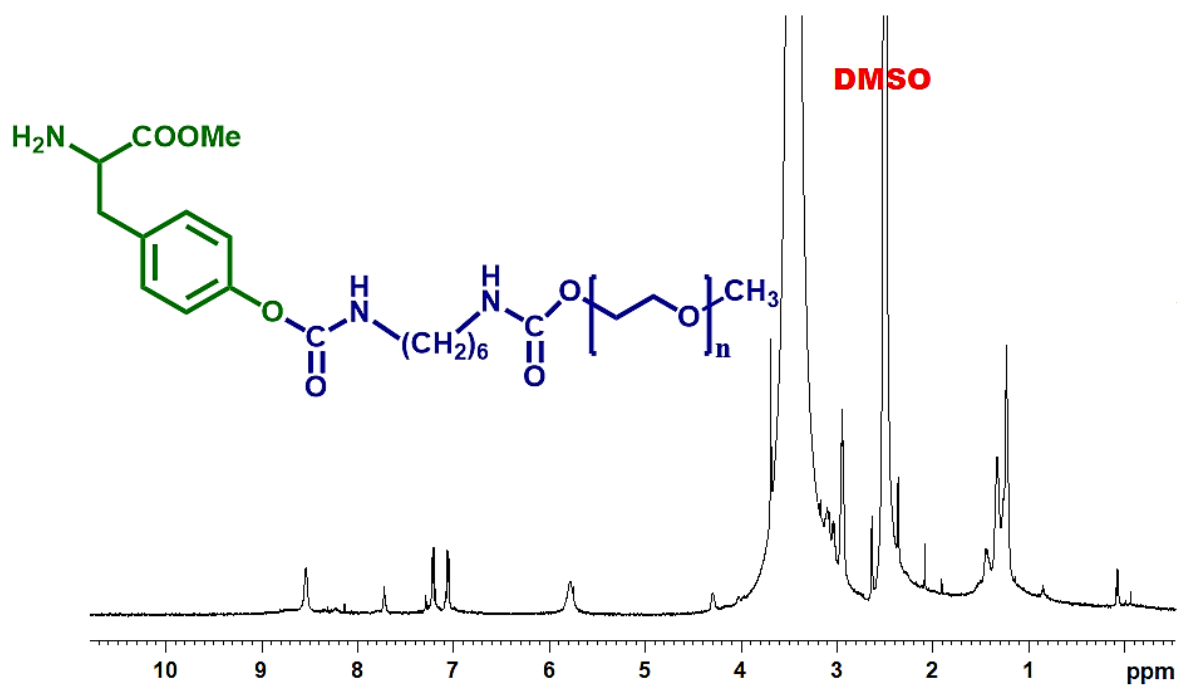
Figure 5.2: ¹H NMR of pre-polymer 2

The deprotection of Boc group of pre-polymer 2 was confirmed by the disappearance of the peak at 1.38 ppm and carbonyl group of Boc group around 1626 cm^{-1} (**Figure 5.2 & Figure S2**). To understand, whether the deprotection occurred under the given reaction conditions, we chose Boc-L-tyrosine methyl ester as model reactant. The reaction was carried out under similar reaction conditions. The reaction was monitored by thin layer chromatography. The product was isolated and confirmed by the GC-MS analysis which showed the amine group was deprotected (shown in **Figure S3).**
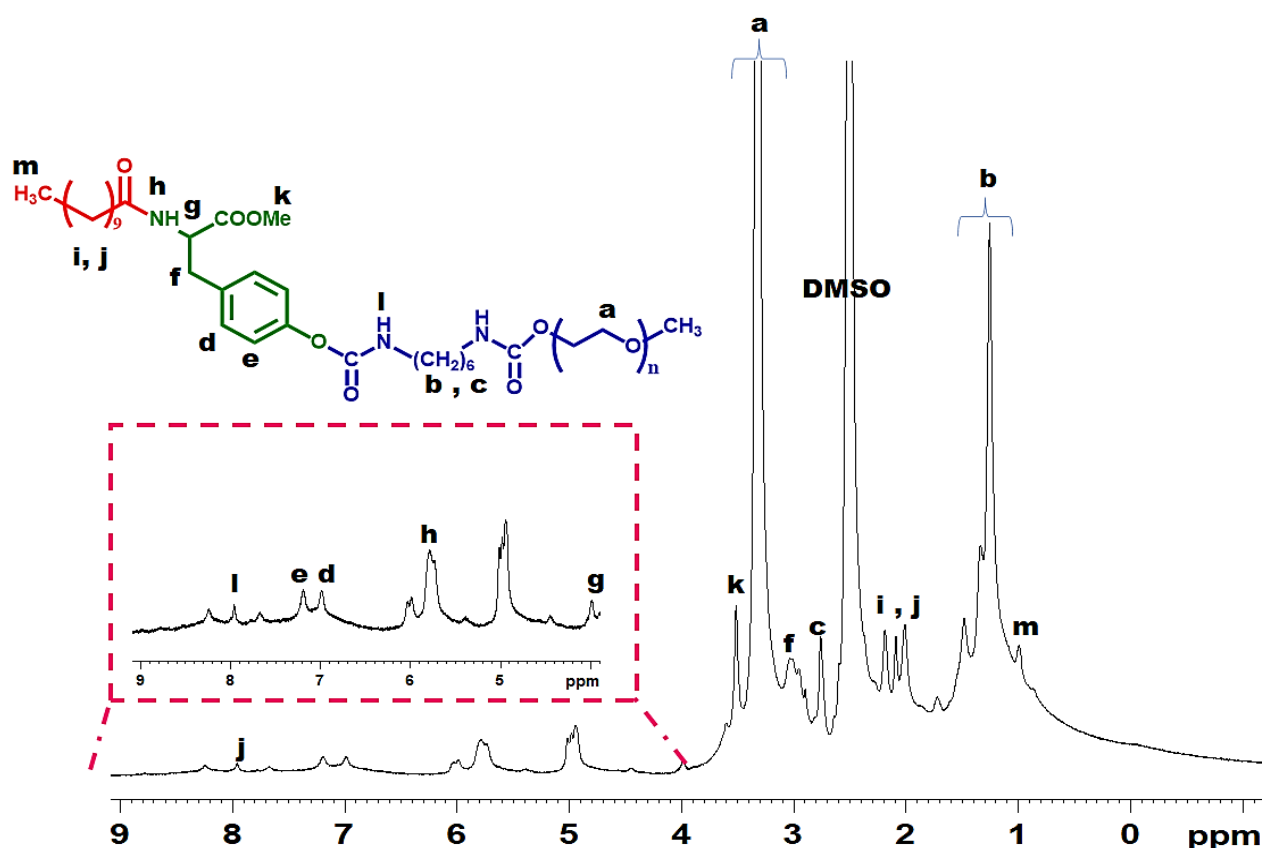
Figure 5.3: ^{1}**H NMR of mPEG and undecanoic acid functionalized tyrosine-derived amphiphilic copolymer**

Undecanoic acid was selected to endow the polymer with a hydrophobic chain. Undecanoic acid was conjugated with the free amino group of pre-polymer 2 using facile 1-Ethyl-3- (3-dimethylaminopropyl) carbodiimide (EDC) chemistry. The amidation was confirmed by FTIR analysis, which showed a carbonyl peak of amide around at 1623 cm^{-1} (**Figure S4**).

The molecular weight (Mn) of the polymer was determined by the ^{1}H NMR end group analysis method. The amphiphilic polymer possesses Mn=7500 g/mol determined by the proton NMR spectrum shown in **Figure 5.3.** TGA analysis of the final amphiphilic polymer revealed that after an initial weight loss, associated with some humidity absorbed, the thermal degradation of side pendant groups and backbone has a well-defined one-step degradation profile in the range of 300-350°C **(Figure 5.4).**
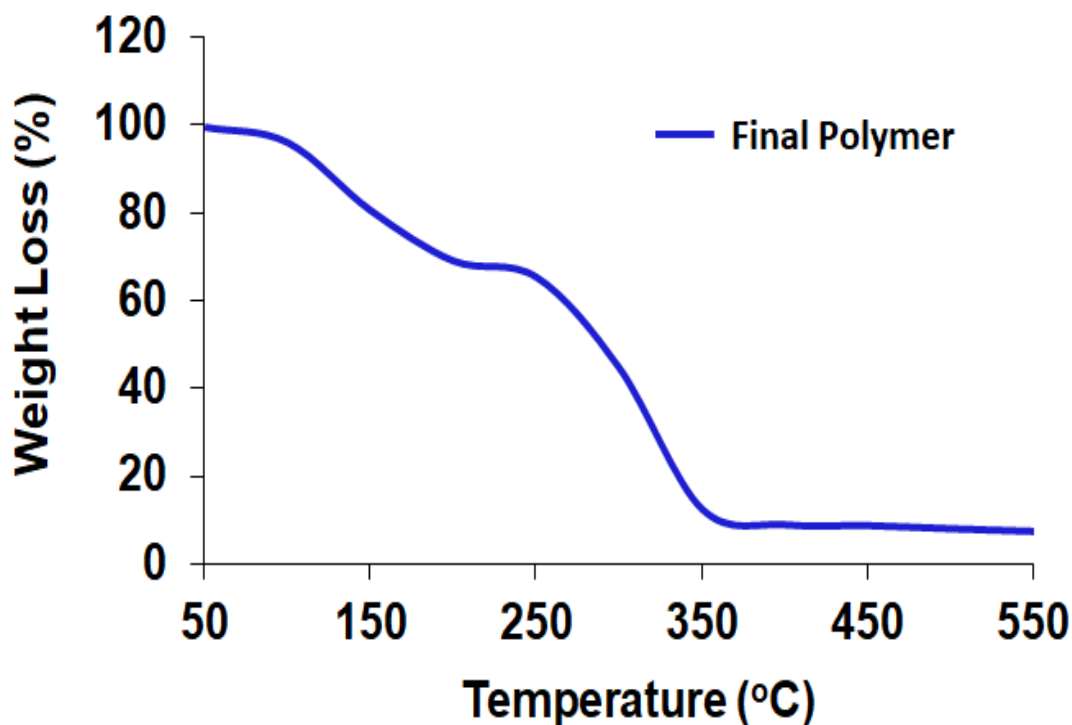
Figure 5.4: TGA profile of final amphiphilic polymer

The synthetic strategy involves the conjugation of a hydrophilic segment and hydrophobic segment via urethane and amide linkage. The topology of a polymer plays a critical role in the properties of the resulting material. Amphiphilic polymers may self-assemble into aggregates with different morphologies, such as micelles, vesicles, rods, and hollow tubes[21]. They have the capacity to display morphological changes by properly adjusting the hydrophilic to hydrophobic ratio (HLB), which is a useful feature to manipulate for applications involving catalysis.

5.3.2 Self-assembly of tyrosine-derived amphiphilic polymer into micelles

The nanomicelles were prepared from the amphiphilic polymer via solvent exchange method. To study the self-assembly of the synthesized amphiphilic polymer, the polymer sample was dissolved in DMSO and subjected to dialysis using semipermeable membrane with molecular weight cut off 3500 Da[22]. The micellar systems showed a uniform size distribution as evident from DLS studies. The hydrodynamic size of the bare micelles was 164 nm **(Figure 5.5).** The HR-TEM imaging also corroborated with the observations of DLS studies demonstrating a homogeneous particle distribution 132 nm **(Figure 5.5).**
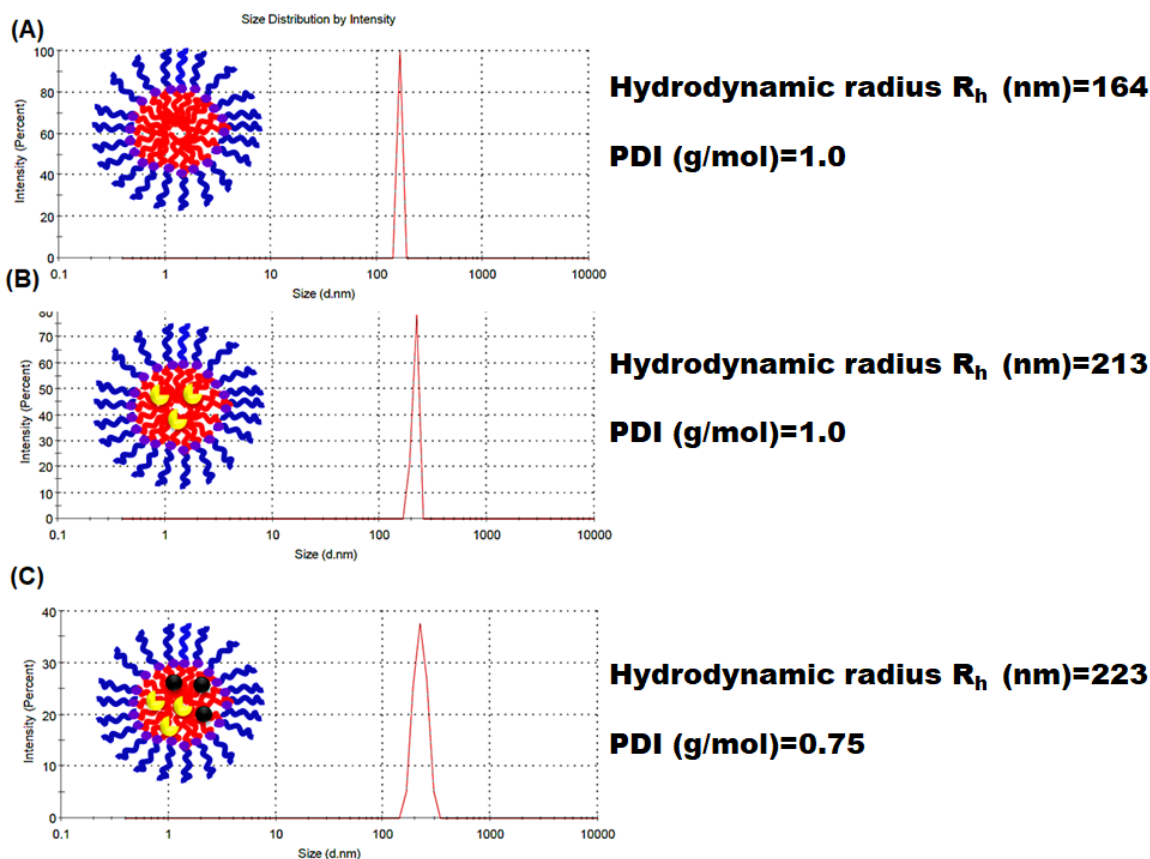
Figure 5.5: Comparison of the size of (A) blank micelles (B) CALB loaded micelles and (C) nZVI and CALB loaded micelles (The samples were maintained at 0.1 mg/mL).

The critical micelle concentration value was determined using a hydrophobic dye, pyrene as a fluorescent probe[23].
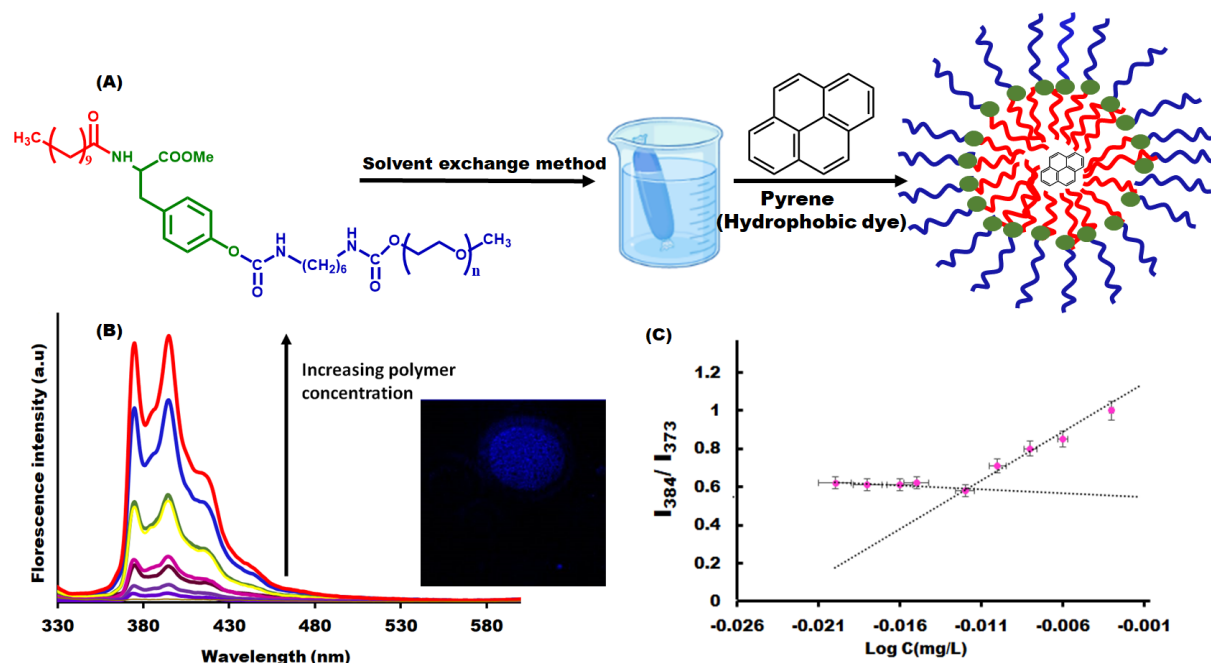
Figure 5.6: (A) Schematic representation of self-assembly of amphiphilic polymer to nanomicelles and subsequent encapsulation of pyrene dye (B) The fluorescence emission spectra of pyrene as a function of polymer concentration (inset: Florescence image of pyrene encapsulated micelles) and (C) The determination of CMC using pyrene as a fluorescent probe. The data were presented as mean ± standard deviation (n=3).

It was observed that, the micelles exhibited low CMC values of 0.97 mg/L (**Figure 5.6**), which indicates that the stability of nanomicelles. This observation is supported by a well-known fact from the literature that the ratio of hydrophobic portion in an amphiphile has an effect on the CMC value. A smaller CMC value is attributed to the higher ratio of hydrophobic counterparts[24]. The higher hydrophobicity of polymer was due to the presence of aromatic ring of tyrosine and methyl groups of undecanoic acid present in the polymer skeleton in addition to the hydrophobicity contribution from methyl groups of HMDI.

The relatively low CMC value make the nanomicelles desirable candidates for catalytic application. Micellar morphology of the tyrosine derived amphiphilic polymer was confirmed by the presence of the hydrophobic core inside the self-assembled amphiphilic polymer. This hypothesis was tested by the fact that the hydrophobic dye molecules can be encapsulated within the hydrophobic interior. The extensively dialyzed solution demonstrated characteristic emission peak of pyrene with λ_{max}

=375-405 nm, indicating successful dye encapsulation. The dye encapsulated solution was examined under the florescence microscope demonstrated single layer blue emitting spherical morphology **(Figure 5.6(b))**.

We have proposed for the first-time successful design and synthesis of nanomicelles co-loaded with CALB and zerovalent iron nanoparticles to act as catalytic nanoreactors. The nanoparticle and enzymes are well dispersed in the hydrophobic core of nanomicelles avoiding any aggregation. The synthesis of biohybrid was initiated by encapsulating CALB (1.2 mg/mL) in amphiphilic polymer derived nanomicelles. The enzyme-loaded nanomicelles solution was dialyzed against PBS buffer (10mM, pH=7) to remove the excess enzyme and evaluate the loaded enzyme quantity in the micelle (**Figure S4**). The enzyme loading in the nanomicelles was 71%, evaluated from the Bradford assay. The hydrodynamic size of the CALB@NM was 213 nm with uniform monodispersity.
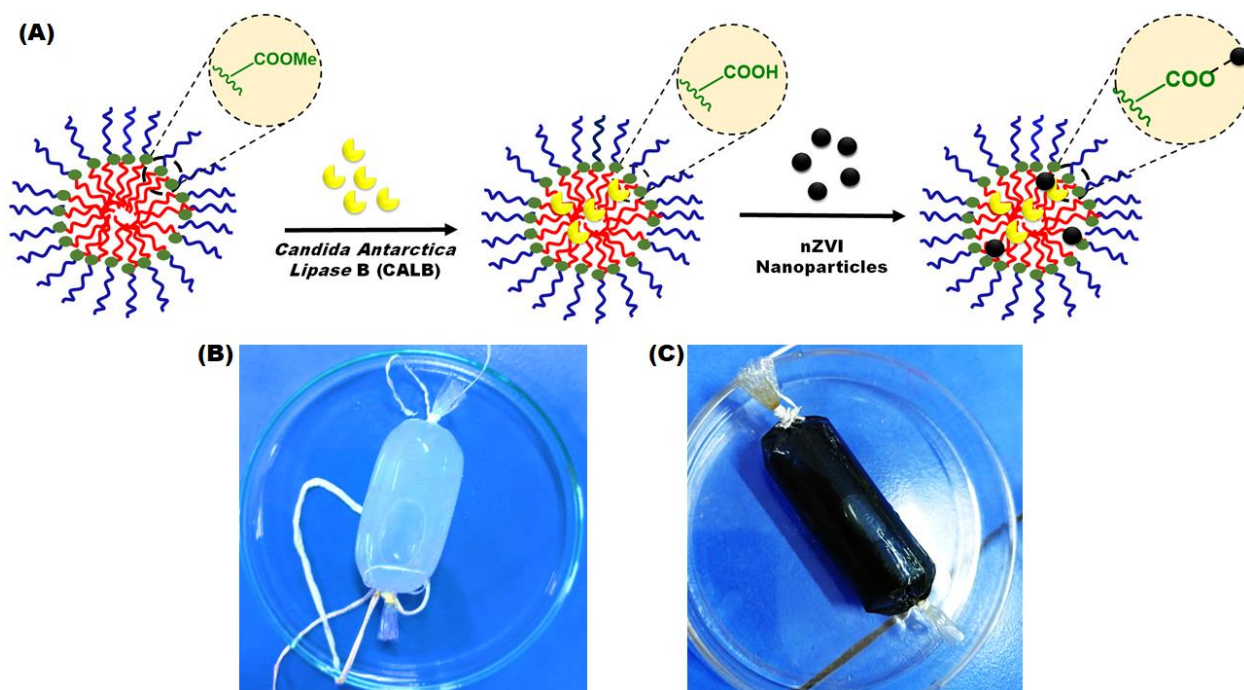
Figure 5.7: Schematic representation of (A) CALB loading in nanomicelles leading to the hydrolysis of ester bond and subsequent loading of nZVI facilitated by free carboxyl groups (B) CALB loading in nanomicelles (i.e, CALB@NM) using dialysis method and (C) nZVI loading in CALB@NM using dialysis method resulting in black coloured uniformly dispersed solutions.

The candida lipase hydrolyses the methyl ester from amphiphilic polymer backbone which results in free carboxylic acid groups which was confirmed by negative value i.e, -14.9 mV obtained by zeta potential analysis of the obtained dialysed solution **(Figure 5.7).** The obtained transparent dialysed solution was added to synthesized zerovalent iron nanoparticles for encapsulation. The carboxylic acids obtained after hydrolysis exists as pendant groups aids in stabilizing iron nanoparticles via electrostatic interactions.

The obtained stable black dispersed solution was dialysed against PBS buffer (10mM, pH=7) to remove excess metal ions. The dialysed solution obtained was used as a catalyst. The loading of zerovalent iron nanoparticles was obtained as 18 wt% analyzed using ICP-AES analysis.

Bare nanomicelles were also characterized by HR-TEM, FE-SEM, AFM. The size of bare nanomicelles was 132 nm as observed from HR-TEM micrographs (Figure5.8(A)). HR-TEM micrographs of the nZVI@CALB without the nanomicelles showed an aggregated chain-like structure, in which the dark field contrast is due to nZVI and light field contrast due to enzyme coating as shown in **Figure 5.8 (D) & 5.8 (E).** HR-TEM micrographs of the catalyst i.e, nanomicelles stabilized CALB and nZVI confirmed the presence of spherical iron nanoparticles (**Figure 5.8(F)**). The size of the iron nanoparticles was found to be in the range of 10-15 nm. Moreover, a light field contrast was due to polymer nanomicelles which stabilized the iron nanoparticles. Notably, it is hard to distinguish the polymer and CALB due to their low contrast under TEM mode. This also suggests that the zerovalent iron nanoparticles remain uniformly dispersed with a spherical morphology as the nanomicelles act as stabilizing agent wherein the carboxyl groups of the polymer network stabilize the nZVI and protect them from agglomeration over a longer period of time. The small size of nZVI leads to a higher surface-to-volume ratio which is advantageous for catalysis.

The slight decrement in the size of HR-TEM measurements as compared to the DLS studies can be attributed to the dehydration of the mPEG chains in the process of sample preparation for the analysis[25]. The polydispersity was more pronounced in the TEM image of the catalyst (i.e, nZVI-CALB@NM) analyzed on dried samples, where drying caused particle aggregation[26]. Despite this fact, the TEM image (**Figure 5.8**) clearly showed iron nanoparticles clustering in spherically shaped hydrophobic cores of the micelles.
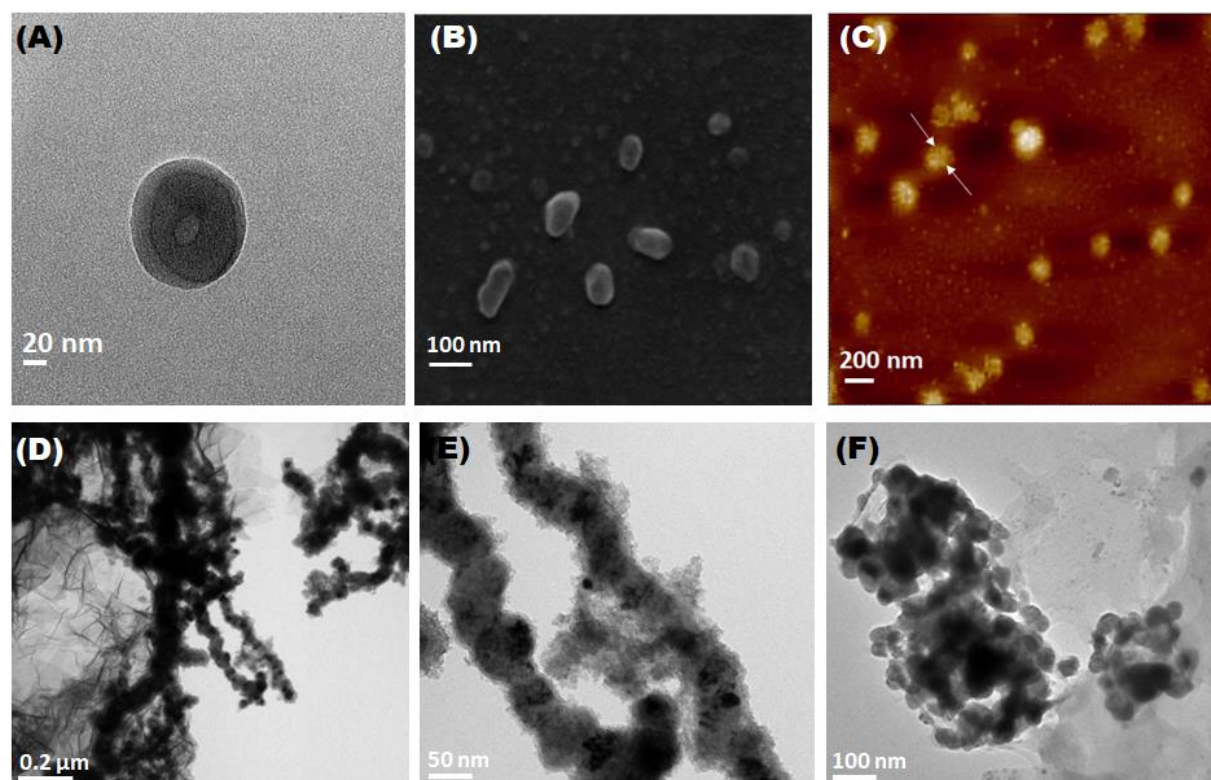
Figure 5.8: Characterization of the self-assembly of tyrosine-derived amphiphile into nano micelles (A) High-resolution transmission microscopy (HR-TEM) image; (B) field emission gun scanning electron microscopy (FEG-SEM) image; (C) atomic force microscopy (AFM) image; HR-TEM images of (D), (E) zerovalent iron nanoparticle and candida lipase B composite (nZVI@CALB); (F) CALB and zerovalent iron nanoparticle co-loaded nano micelles (The samples were maintained at 1 mg/mL concentration for the above mentioned characterizations).

The surface composition of the catalyst was investigated by the XPS analysis. A complete scan from 0 to 1000 eV binding energy demonstrated the presence of C, O, N, and Fe elements for the catalyst as shown in **Figure 5.9**. For XPS analysis, the catalyst was dried and then analyzed. Deconvulated spectra of all the elements have been shown in **Figure 5.10.** In the XPS analysis the photoelectron can penetrate ~5 nm deep from the surface, and the Fe^0 peak observed demonstrated very low intensity. The intensity of Fe^0 peak was found to be lower compared to the peaks of Fe2p3/2 at 712.5 corresponding to the Fe (III) such as Fe_2O_3 & FeOOH and 719.1 corresponding to the overlap of oxidized iron and zero-valent iron nanoparticles[15]. This can also be attributed to the oxidation of nZVI during the drying process. Thus, the low binding energy 705 eV

corresponding to Fe (0) was obtained consistent with the literature report[27]. The binding energy corresponding to the C 1s of C-C and O-C=O linkages was observed at 284.8 and 288.6 eV respectively. The binding energy for O 1s was observed at 532 eV corresponding to C-O linkage and 535 eV attributed to the metal oxide binding energy[28]. The binding energy for N 1s was observed at 399 eV, attributed to the O=C-N linkage. The presence of carbon, oxygen, and nitrogen was observed due to the polymer nanomicelles in the catalyst composition.
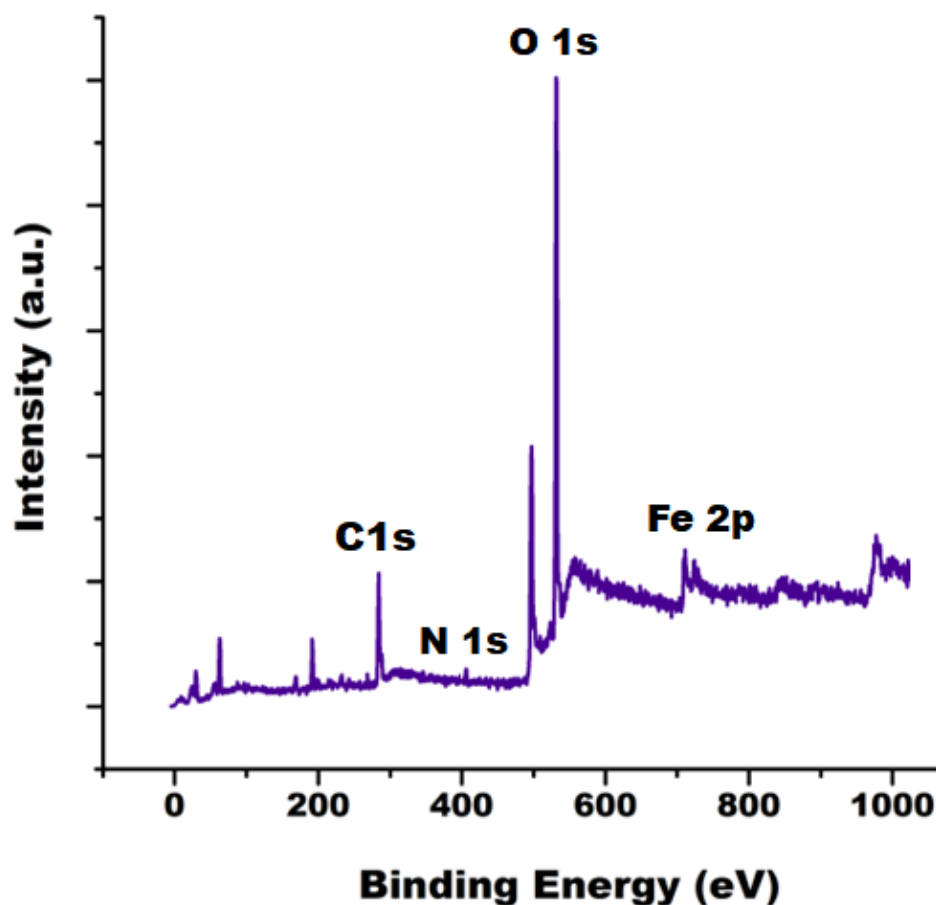
Figure 5.9: Full scan XPS spectrum of nZVI-CALB@NM (solution was dried into powder form).
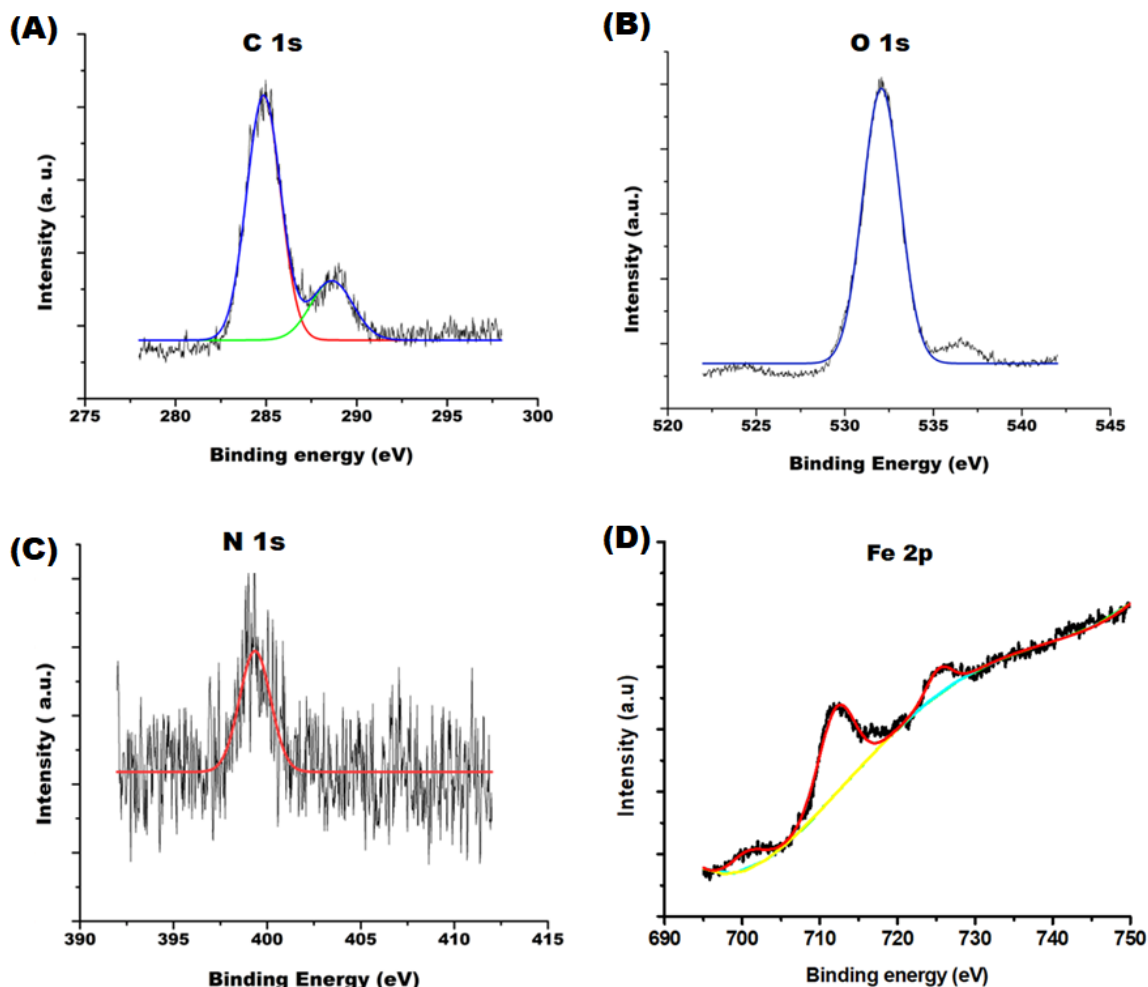
Figure 5.10: Deconvulated spectra of nZVI-CALB@NM (A) C 1s (B) O 1s (C) N 1s and (D) Fe 2p.

To evaluate the magnetic property of the loaded zerovalent iron nanoparticles, VSM analysis was carried out. The magnetic hysteresis curve is shown in **Figure 5.11**. The magnetization values were calculated 24 emu g^{-1}. Thus, confirming the superparamagnetic property which is also evident from an easy separation using an external magnet.

To check the structure stability of native enzyme and enzyme loaded in catalyst, circular dichroism analysis was carried out. The CD spectra of CALB and nZVI-CALB@NM revealed that the structure of enzyme was almost identical, which showed that the overall confirmation of the CALB is intact during the catalytic nanoreactors synthesis[29]. However, two spectra showed minor deviations which can be due to some local confirmational changes (**Figure 5.12**).
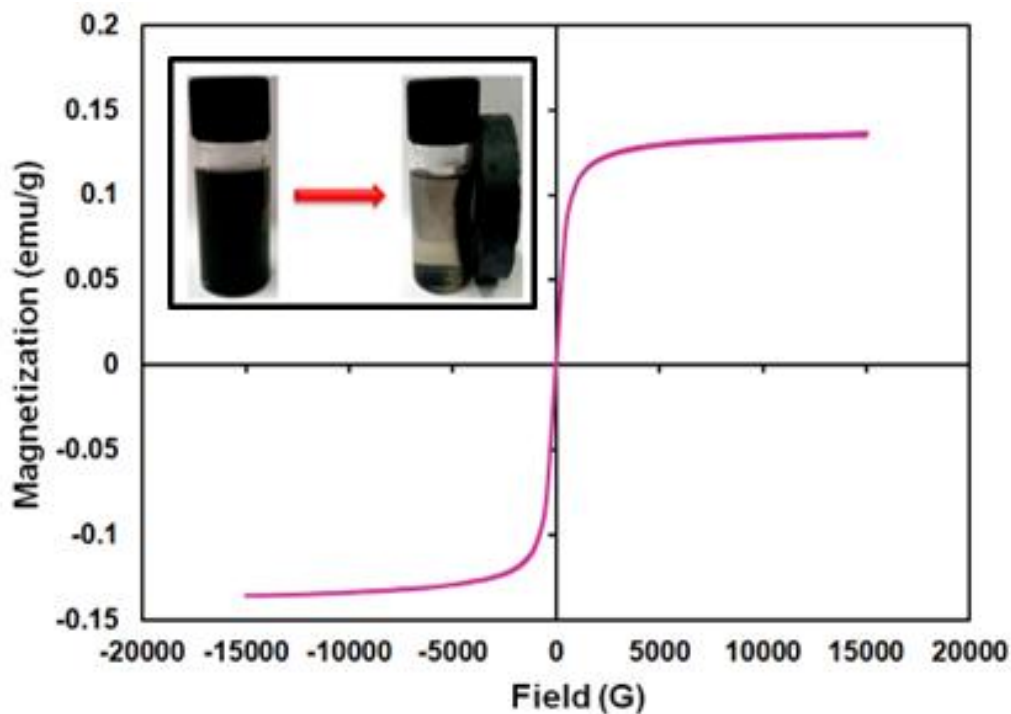
Figure 5.11: Evaluation of magnetic property via room-temperature magnetization curve
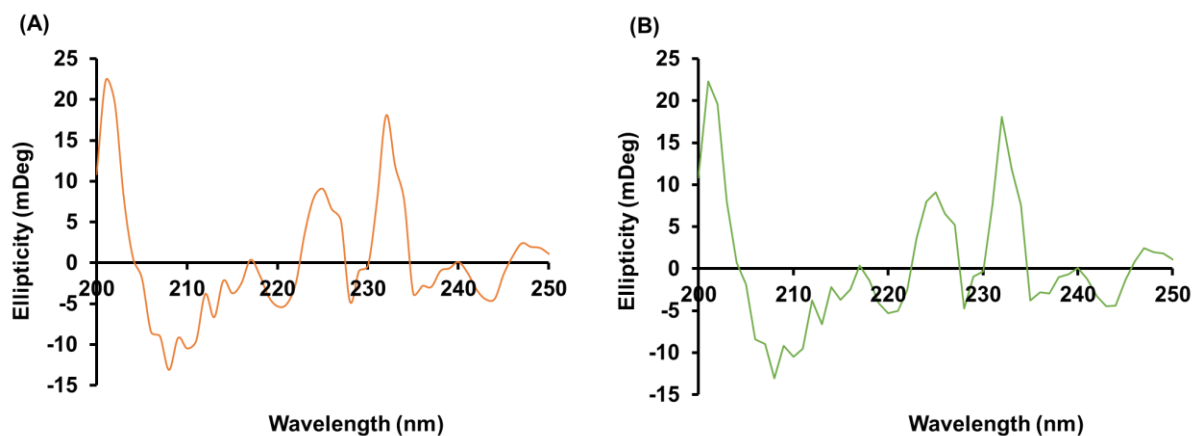
Figure 5.12: CD spectra of (A) Free CALB and (b) nZVI-CALB@NM.

5.3.3 Catalytic evaluation of nZVI-CALB@NM for chemoenzymatic cascade reaction

As shown in Scheme 2, the cascade reaction consists of two steps, the first step is the hydrolysis of p-nitrophenyl acetate (p-NPA) by CALB to form p-nitrophenol (p-NP) as an intermediate, and the second step is the reduction of p-nitrophenol (p-NP) to p-aminophenol (p-AP).
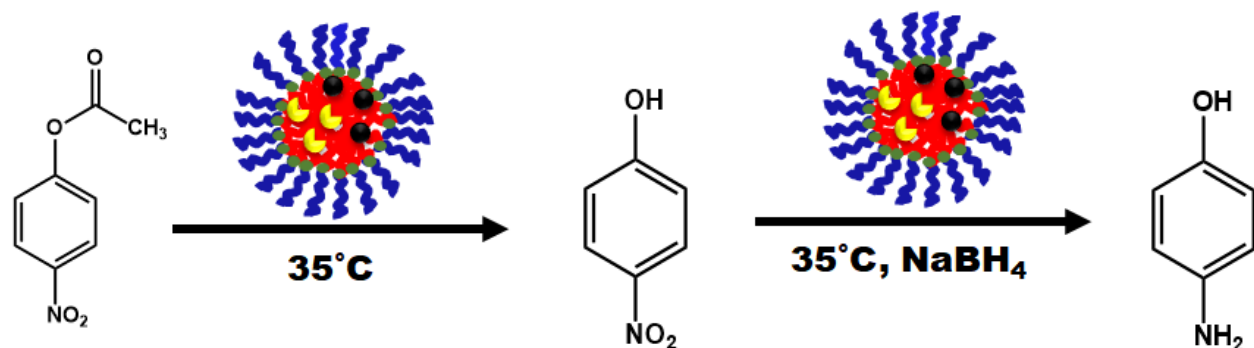
Scheme 5.2: Schematic representation of chemoenzymatic cascade reaction in presence of nZVI-CALB@NM.

To evaluate the activity of nZVI-CALB@NM towards the chemoenzymatic cascade catalysis, we first investigated the hydrolytic and hydrogenation activities, separately, as shown in Figure 6. p-Nitrophenyl acetate was used as a model substrate for the measurement of the hydrolytic activity of nZVI-CALB@NM. The release of p-nitrophenol (p-NP) from p-nitrophenyl acetate (p-NPA) due to hydrolysis was observed for 30 min. With the increase in time, the concentration of p-NP increased (in terms of peak at 405 nm, p-NP has maximum absorbance at 405 nm), which shows the hydrolysis step took place successfully in presence of the CALB. However, no new peak occurred around 312 nm corresponding to p-aminophenol (p-AP), which indicates that the nanoreactors is not capable of reducing the p-NP further to p-AP by itself. Hence, a reducing agent is required for the successful cascade synthesis of 4-AP.

The reduction step in presence of nZVI-CALB@NM and mixture of CALB and nZVI was carried out using sodium borohydride as reducing agent. The decrease in absorbance at 405 nm and appearance of new peak at 312 nm shows the formation of p-AP from p-NP. The reaction rate constant (k) was determined from the absolute value of the slope using the equation 2 and conversion of 4-NP to 4-AP using equation 3.

These results clearly demonstrate the ability of catalytic nanoreactors to catalyze the hydrogenation step successfully. The k value was 15.8 X 10^{-2} min^{-1}, when the reaction was catalysed in presence of nZVI-CALB@NM and in presence of CALB and nZVI mixture as catalyst, the k value was 2.65 X 10^{-2} min^{-1} (**Figure 5.13**). The conversion was excellent and monitored using UV-visible spectroscopy. As expected, in presence of nanomicelles, the CALB and zerovalent iron nanoparticles synergistically behave as catalytic nanoreactor, with small size and less aggregates. nZVI-CALB@NM gave a higher catalytic activity compared to simple CALB and nZVI mixture

in the absence of micelles. Indeed, the presence of nanomicelles positively impacted outcome of the reaction, leading to faster reaction rate.
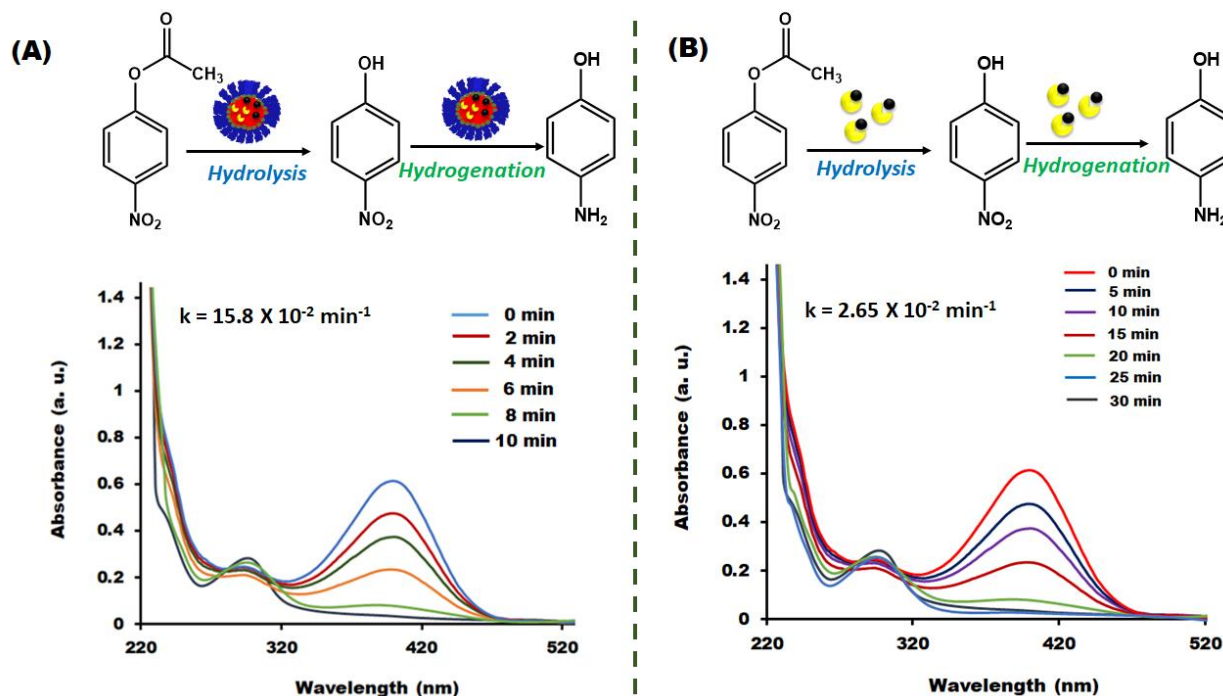

Figure 5.13: Hydrolysis of p-nitrophenylacetate in presence of (A) nZVI-CALB@NM and reaction kinetics of the hydrogenation step (B) CALB and nZVI mixture and reaction kinetics of the hydrogenation step (Reaction conditions: p-NPA (1 mM), Catalyst (2 mL contains nZVI (18 wt%), NaBH$_4$ (1.4 mM) at 35°C).

After evaluating the hydrolytic and hydrogenation activity separately, it was established that both CALB and nZVI are required for the cascade synthesis of 4-AP. nZVI-CALB@NM was subjected to the chemoenzymatic cascade reaction for converting p-nitrophenyl acetate (p-NPA) to p-aminophenol (p-AP) in presence of sodium borohydride in a single pot. Therefore, the nanoreactors composed of CALB and nZVI stabilized in core of the nanomicelles can catalyze the cascade reaction effectively. The hydrophobic interactions between the reactant and hydrophobic core of the nanoreactors and the close proximity between the reactant and catalyst leads to effective catalysis in water under ambient conditions. It indicates that the high surface area, better dispersibility and the nanostructure of nZVI in the nZVI-CALB@NM might contribute to the high catalytic activity.

5.3.4 Aqueous nanomicellar solutions as the reaction medium.

We have investigated the chemoenzymatic cascade synthesis of p-AP from p-NPA under different reaction conditions. The p-nitrophenylacetate was used as the model substrate. As shown in Table 5.1, the volume of catalyst was varied from 0.5 mL to 5 mL using sodium borohydride 2 mM with 1 mM p-NPA substrate concentration. For the cascade reaction, the time taken was 40 mins and 35 mins when 0.5 and 1 mL catalyst was employed respectively (Table 5.1, entry 1-2).

When we increased the catalyst volume to 2 mL, the time required for the reaction completion was 20 mins. Beyond 2 mL of the reaction time did not change (Table 5.1, entry 4-5). Remarkably, enzymatic superactivity to hydrolyse 4-NPA is observed when the 2 mL of micelle solution was used for the reaction. These results confirm that increasing the catalyst volume in aqueous medium helps to moderate enzyme saturation, which assists efficient catalysis.

Hence, the catalyst volume was fixed to 2 mL for further optimizations. Furthermore, the hydrogenation step was performed using a different concentration of $NaBH_4$ in the standard reaction. When we decreased the concentration of $NaBH_4$ from 2mM to 1.6 mM the reaction time did not change (Table 5.1, entries 5-11), whereas using 1.4 mM of $NaBH_4$ resulted in a remarkable yield 96% at 35 °C and reaction time i.e, 26 minutes (Table 5.1, entry 8). However, further lowering the amount of $NaBH_4$ to 1.2 mM caused an increase in the reaction time (Table 5.1, entry 9) and hence an adequate concentration of $NaBH_4$ (1.4 mM) was used for the optimum reaction conditions.

Further we increased the iron loading in the nanomicelles by increasing the molarity of the iron salts from 0.1 M to 0.5 M. It was observed that the reaction time decreased with increasing iron loading, as shown in Table 5.1, entries 9-14. These observations suggest the optimized reaction conditions involves the appropriate amount of iron loading using 0.3 M of iron salt, the reaction time was 10 mins with 1.4 mM $NaBH_4$ and 2 mL catalyst loading (Table 5.1, entry 12). On further increase of iron loading, no appreciable change in reaction time was observed. While carrying out dialysis, it was observed that, when iron loading was increased from 0.3 M to 0.5 M, the solution outside the dialysis bag turned yellow, due to release of excess of iron in the nanomicelles. It means the maximum capacity of nanomicelles to encapsulate nZVI was 0.3 M. The concentration of nZVI loaded was found to be 18 wt% using ICP-AES analysis. Further, under the optimized reaction conditions, the substrate concentration of p-NPA was increased from 1 mM to 10 mM. The reaction time for 1 mM, 5 mM and 10 mM was 8, 12 and 20 mins respectively. Thus, nanoreactors in the

buffer help to regulate the amounts of both the substrate and the product in an aqueous media by providing a controlled supply that does not overload the enzyme enabling greater conversion rates.

Table 5.1: Optimization of reaction conditions for the chemoenzymatic cascade catalysis for the synthesis of p-aminophenol using p-nitrophenylacetate as a model reactant
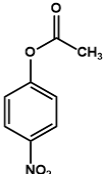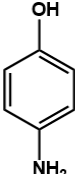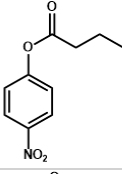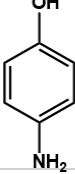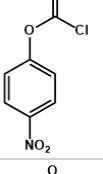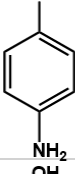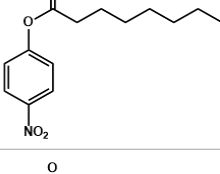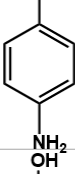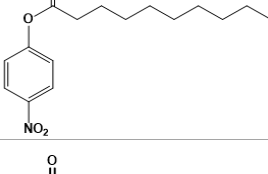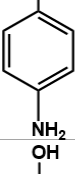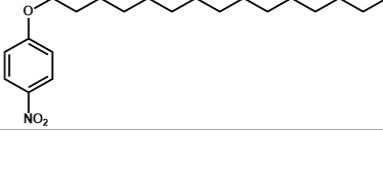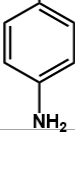
Sr.No.	Volume of catalyst (mL)	Conc. Of NaBH$_4$(mM)	Conc. Of Fe (M)	Conc. Of p-NPA (mM)	Time (min)
1.	0.5	2	0.1	1	40
2.	1	2	0.1	1	35
3.	2	2	0.1	1	20
4.	3	2	0.1	1	20
5.	5	2	0.1	1	18
6.	2	1.8	0.1	1	25
7.	2	1.6	0.1	1	26
8.	2	1.4	0.1	1	26
9.	2	1.2	0.1	1	30
11.	2	1.4	0.2	1	15
12.	**2**	**1.4**	**0.3**	**1**	**10**
13.	2	1.4	0.4	1	10
14.	2	1.4	0.5	1	8
15.	2	1.4	0.3	5	12
16.	2	1.4	0.3	10	20

Reaction conditions: All the reactions were carried out at room temperature (35 ˚C).

After optimization of the reaction conditions, we subsequently extended the scope of the nZVI-

CALB@NM with a variety of p-nitrophenyl esters. The kinetics was performed for the hydrogenation step for every substrate, similar to the 4-NPA protocol mentioned above.

Table 5.2: Substrate scope was extended to p-Nitrophenyl esters of fatty acids with different chain length tested of the reaction under the optimized condition using nZVI-CALB@NM.

Sr.No.	Substrate	Product	Time (min)	%Conversion
1.			20	98
2.			22	96
3.			35	95
4.			43	96
5.			45	98
6.			50	99

Reaction conditions: Substrates (1 mM) Catalyst (2 mL, contains nZVI (18 wt%)), NaBH$_4$ (1.4 mM) at 35°, % Conversion was calculated for the hydrogenation step using UV-Visible Spectrophotometry.

The catalytic performance of the nanomicellar catalyst was significantly influenced by the nature of the substituent on the nitroaromatic compound. p-Nitrophenyl esters with a long chain (Table 5.2, entries 4-6) require longer reaction times compared to the esters with a short chain substituent which can be due to the size of the substrate. All the nitrophenylesters were reduced in good to excellent yield affording a single product, which minimizes the efforts to separate the unreacted starting materials. The UV-visible spectra of all the compounds are shown in **Figure S6**.

Thus, nanomicelles in the buffer help to control both substrate and product concentrations in an aqueous medium, this provides a controlled supply of the substrate and that will not overwhelm the enzyme and the nanoparticles, thereby allowing for higher rates of conversion[30].

5.3.5 Synthesis of acetaminophen via sequential tandem catalysis in one pot.

Several attempts have been made for the paracetamol synthesis by employing different routes as shown in Figure 5.14.
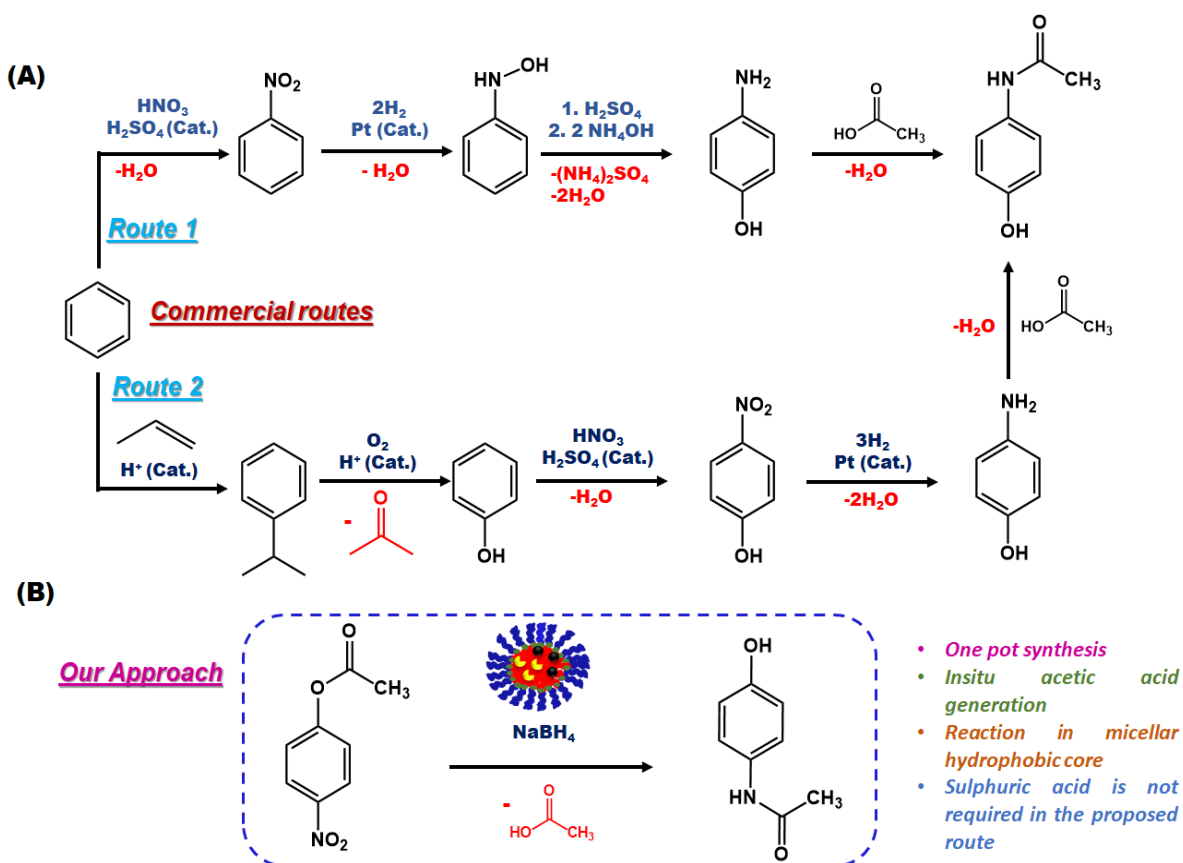

Figure 5.14: (A) Commercial routes for acetaminophen synthesis (B) Our approach for the direct synthesis of acetaminophen.

Generally, the commercial routes involves benzene as starting material, nitration step which is associated with the unwanted formation of ortho aminophenol in significant amount. Morever, expensive platinum metal is required as catalyst for the hydrogenation step. Furthermore, many attempts have been made for the replacement of corrosive and polluting sulphuric acid, but the results obtained are low selectivities[31].

Some of the research groups have reported the synthesis of acetaminophen by employing different strategies. For instance, Gopinathan et al. have previously shown a chemical route to synthesize acetaminophen with 86% yield from the reaction of hydroquinone with an acetamide at elevated temperatures (280− 300 °C) in the presence of solid acid catalysts such as zeolite β or a heteropolyacid[32]. A green chemical route was proposed by Joncour and Coworkers for direct synthesis of acetaminophen with high yield (95%) from hydroquinone using ammonium acetate as an amidating agent, but the reaction was carried out at high temperature (220 °C) and long reaction time (15 h)[31]. Sun et al. reported a bioinorganic nanohybrid catalyst made with a combination of esterase and platinum nanoparticles for the acetaminophen synthesis in 10 mins with 96% yield [28]. Inspired by above report, we have developed a novel catalytic nanoreactors by combining CALB and nZVI in the tyrosine derived nanomicelles for the direct synthesis of p-acetaminophen from p-nitrophenylacetate in aqueous medium at room temperature. The nanoreactors in aqueous medium not only act as reaction medium but also as solvent.

We have tested the combined catalytic activities of CALB and nZVI in nanomicelles using 4-nitrophenyl acetate as starting material in a single pot. When the catalyst was incubated with 4-nitrophenyl acetate, $NaBH_4$, and acetic acid, the final product, acetaminophen, was spontaneously formed in the reaction flask. All reactions were performed in a single flask at room temperature without any specialized equipment. The reaction started in an aqueous phase, but subsequent hydrolysis of 4-nitrophenylacetate by nZVI-CALB@NM led to the formation of acetic acid as by product. Hydrolysis in nanoreactors hydrolysis yielded 4-nitrophenol as an intermediate, with the development of a yellow-coloured solution (**Figure 5.15**). Subsequent reduction of 4-nitrophenol was monitored by the disappearance of the yellow colour under reducing reaction conditions, showing that this two-step reaction was completed by single nanobiohybrid catalytic platform. The hydrogenated product, 4-aminophenol, undergoes acetylation, subsequently reacted with acetic acid in the micellar medium to form the final product, acetaminophen ((N-(4-hydroxyphenyl) acetamide)). The progress of reaction was monitored using UV-visible spectrophotometry.
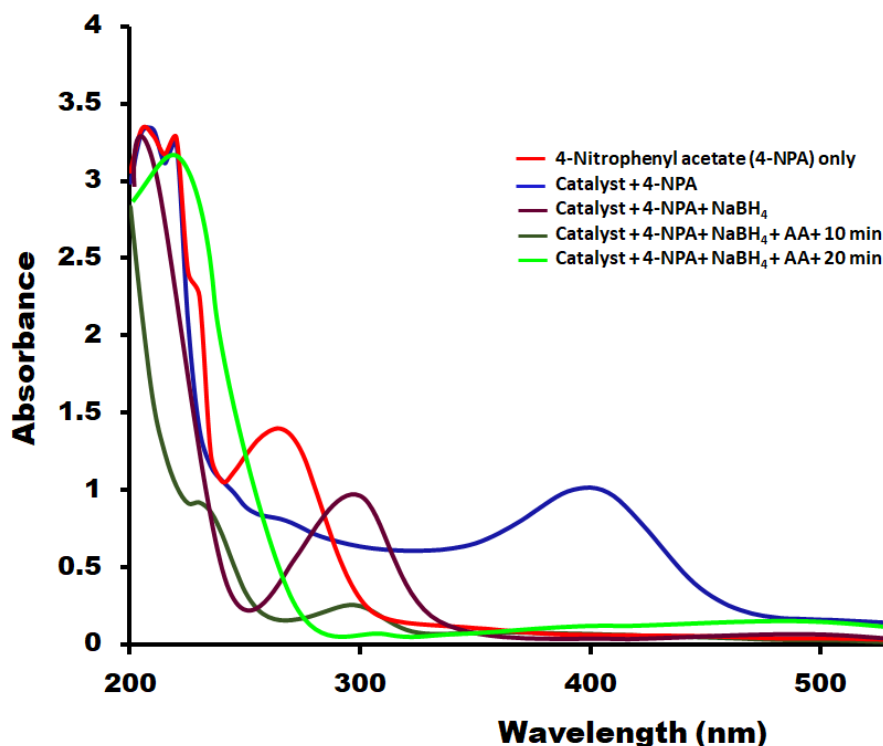
Figure 5.15: Graphical representation showing the control reactions to establish the role of nZVI-CALB@NM in the cascade reaction (Reaction conditions: p-NPA (1 mM, Catalyst (2 mL contains nZVI (18 wt%), NaBH4 (1.4 mM) at 35°C).

Therefore, the aqueous phase possesses an acidic pH. However, because it is known that acetylation can be carried out in the presence of weakly acidic environments, the entire reaction can be carried out without the use of any additional organic solvent.

For the same reasons, the whole cascade process occurred in a single pot, isolation of products and byproduct is not necessary before acetylation. The whole reaction process was completed within 30 min because no spectral change was observed after 30 min of reaction. Further, we have scaled up the process and isolated the final compound after the reaction completion.

The isolated product was characterized by analytical techniques such as NMR, FT-IR and GC-MS analysis (**Figure 5.16 – 5.18**). All the analysis confirmed acetaminophen as the product obtained from p-nitrophenylacetate in excellent yield (>98%). These benefits can and will result in significant cost reductions for the sector. As a result, this technique might make it easier to produce pharmaceutically active molecules in a setting where funding for a new production line or access to equipment is limited.
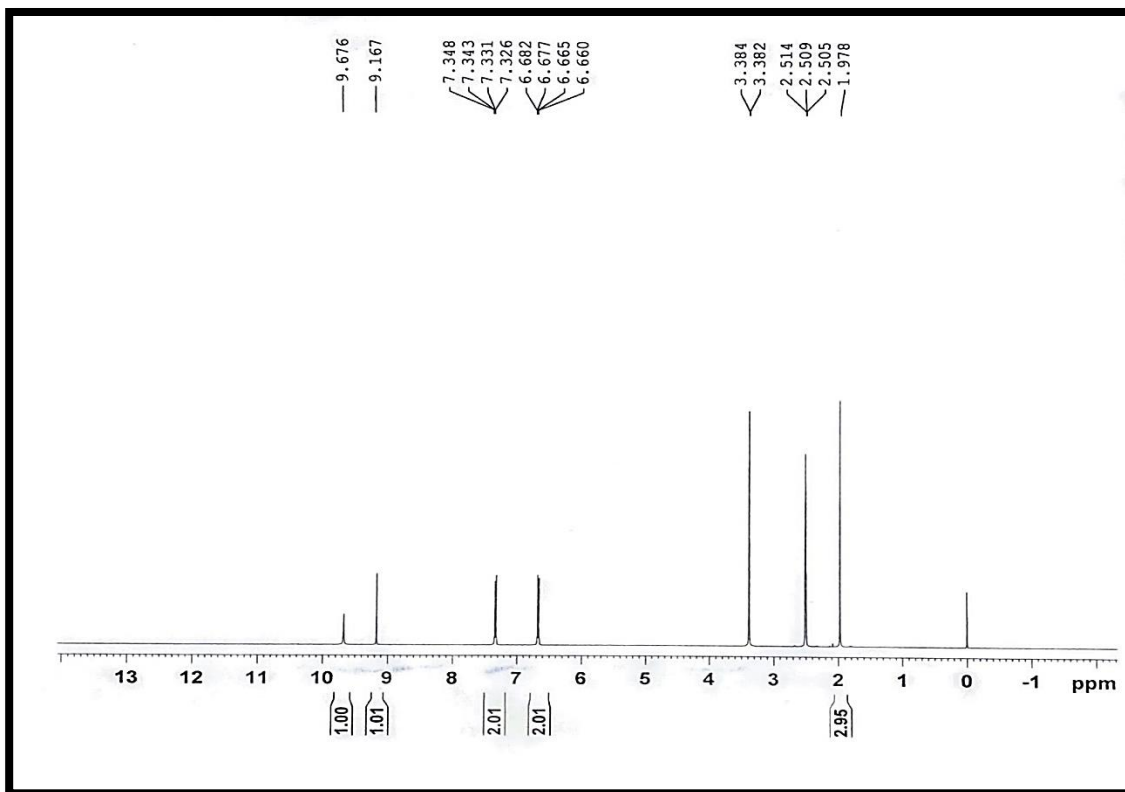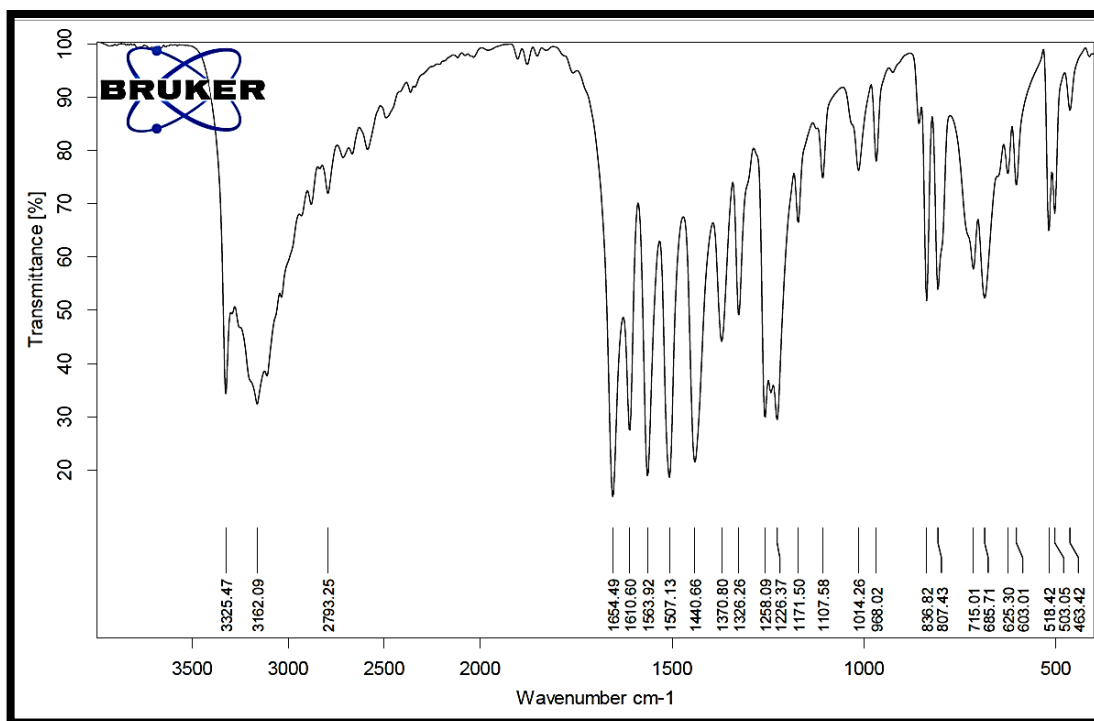
Figure 5.16: ¹H NMR of p-acetaminophen

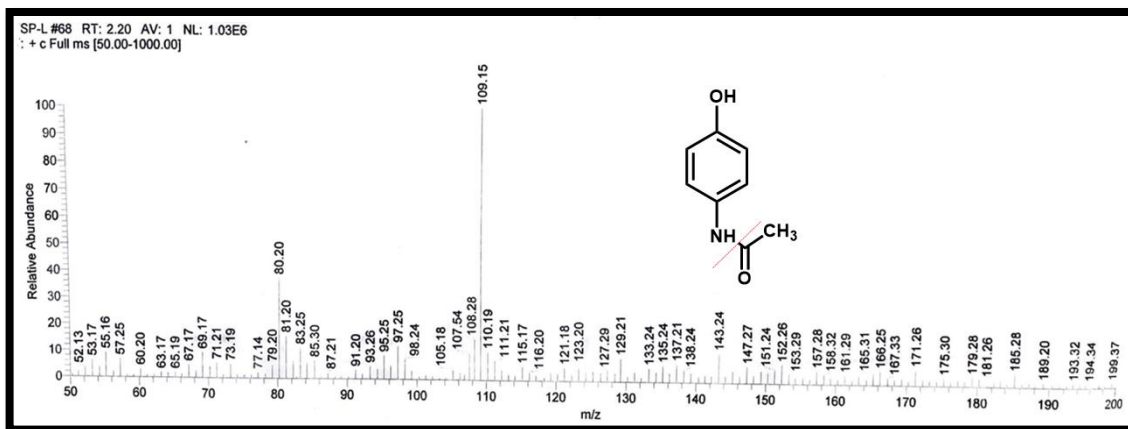**Figure 5.17: FTIR of p-acetaminophen**

Figure 5.18: Mass analysis of p-acetaminophen

5.3.6 Recycling studies

The catalytic nanoreactors demonstrate another advantage, i.e, recyclability. It was also established from the recycling experiments that hydrogenation activity did not decrease even after multiple cycles and the catalyst was very stable for 5 cycle **(Figure 5.19).** After the reaction completion, nZVI-CALB@NM were separated from the reaction mixture via magnetic decantation. The product was analyzed by uv-visible spectrophotometry. HR-TEM imaging of the recycled catalyst after the 5th cycle showed a change in micellar morphology and slight agglomeration of zerovalent iron nanoparticles. FE-SEM analysis also showed some aggregated nanomicelles. The recycling results also demonstrated that the catalyst has not been deactivated. It is very well-established fact that leaching and deactivation of catalyst have a cause-effect relationship[33].
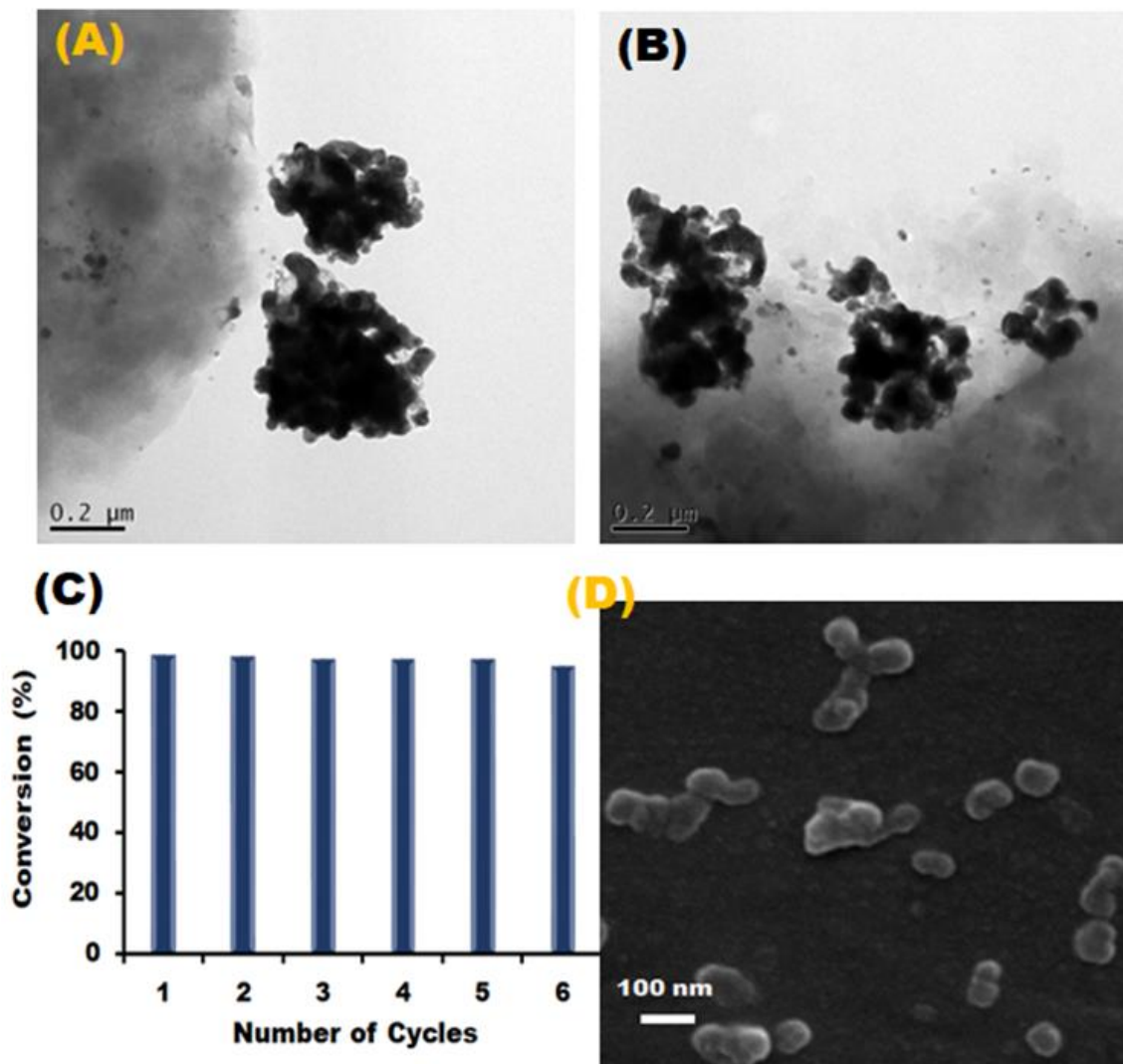
Figure 5.19: (A), (B) HR-TEM image of the recycled catalyst after 5th catalytic cycle, (C) recycling study and (D) FEG-SEM analysis of the recycled catalyst.

To confirm that no leaching occurred, we have dialyzed the reaction mixture using dialysis membrane with 3500 Da molecular weight cut off and dialysis solvent (milli q water) was analyzed by ICP-AES analysis. It was confirmed from the ICP-AES analysis that Fe ion was not detected in the dialysis solvent. Therefore, we can say that there was no leaching occurred in the current experimental setup.

5.3.7 Plausible Mechanism

A plausible mechanism was proposed to explain the phenomenon of catalysis as shown in **Scheme 5.3.**
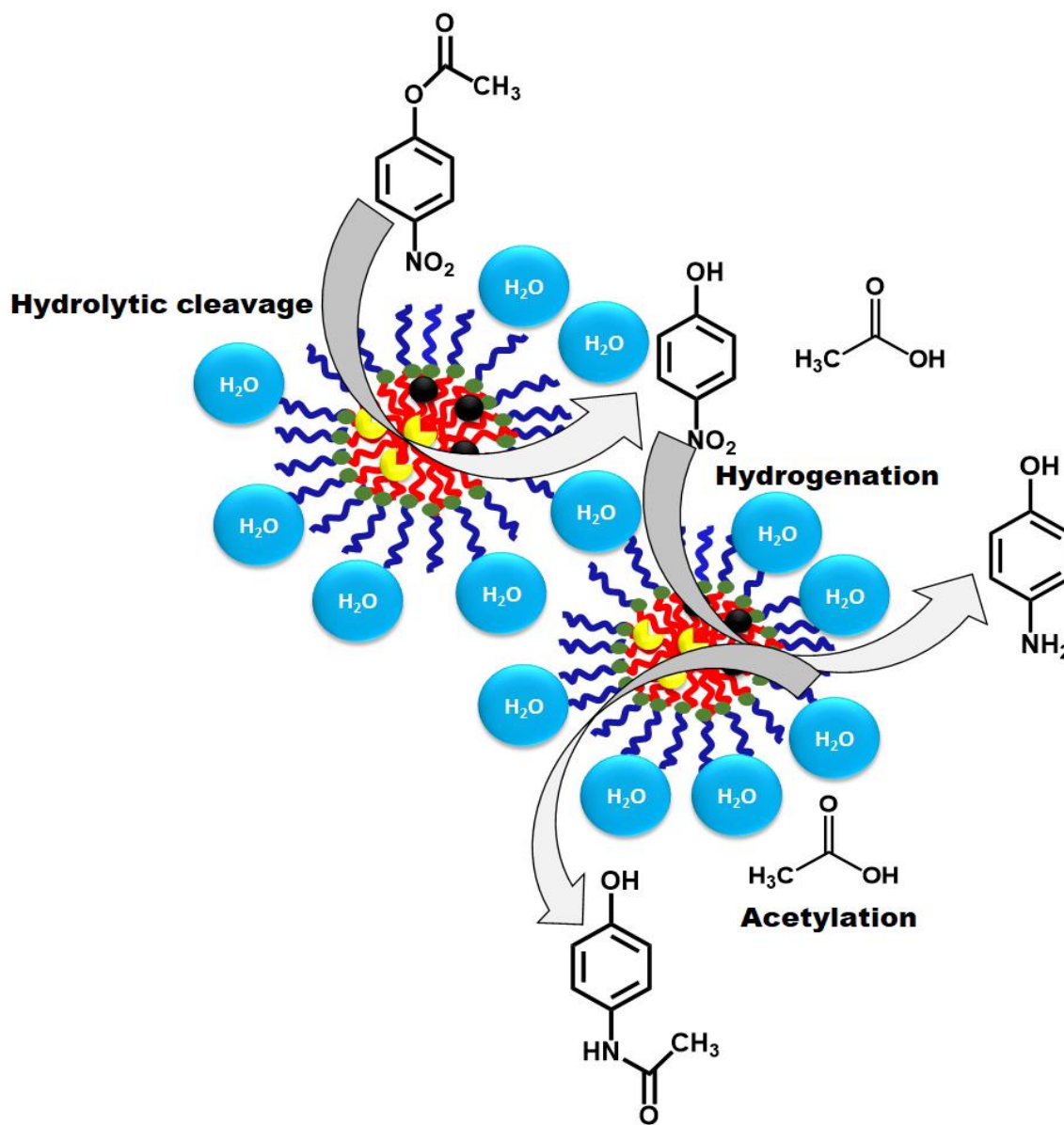
Scheme 5.3: Plausible mechanism for the direct synthesis of acetaminophen using 4-nitrophenyl acetate as reactant in the nanomicelle core.

nZVI-CALB@NM acts as catalytic nanoreactors for the cascade organic transformation. These nanoreactors can entrap the reactants by the virtue of hydrophobic interactions and thus the reactions can be carried out in water instead of organic solvents. The fluorescence microscopy image of hydrophobic dye (i.e, pyrene) encapsulated in micelles provides evidence for their ability to entrap hydrophobic moieties (**Figure 5.6**). The nanoreactors contains CALB and catalytically

active zerovalent iron nanoparticles. Due to confinement of both enzyme as well as nZVI in the nanomicellar hydrophobic core, the hydrophobic reactant molecules come in close proximity with enzyme and nZVI. Herein, the *insitu* generated acetic acid facilitates the acetylation step and also keeps the weakly acidic medium.

5.4 Conclusion

A novel amphiphilic polymer was successfully synthesized by functionalization of tyrosine with polyethylene glycol and undecanoic acid. The amphiphile self-assembled into nanomicelles with a low CMC value of 0.97 mg/L, that indicated the high stability of nanomicelles. These nanomicelles were used for stabilizing the CALB and nZVI nanoparticles in the hydrophobic core, to obtain catalytic nanoreactors. We have proposed the environmentally benign chemoenzymatic cascade reaction of p-nitrophenylesters to p-aminophenol using the rationally designed catalytic nanoreactors in water at ambient reaction conditions. The environmentally benign chemoenzymatic cascade reaction was proposed for the multistep catalytic synthesis of the acetaminophen from p-nitrophenyl acetate under the optimized reaction conditions, the final product was obtained in good yield in 30 min. This process avoids the use of toxic solvent, expensive metals and hazardous acid. The acetic acid generated *in situ*, provides mild acidic condition for the synthesis of acetaminophen. The catalytic synthesis of acetaminophen was scaled up and the product was isolated and characterized using ^{1}H NMR, FTIR and ESI-MS spectroscopic techniques.

To demonstrate the robust nature of the nanoreactors, a series of p-nitrophenyl ester derivatives were used as reactants for the cascade reactions. The corresponding p-aminophenol was obtained as desired product under mild reaction conditions in reasonable reaction time. Finally, the operational recyclability showed no significant loss in activity up to 5 consecutive cascade cycles of use at 35˚C. The easy magnetic recovery and reusability of the catalytic nanoreactors is critical for their application in scale-up processes. From this work, we envisage the enzymatic and heterogeneous catalysis can be combined in nanomicelles to create novel cascade industrial manufacturing processes. These findings also imply that similar results can be anticipated for other enzymatic processes and sequential cascade catalysis.

5.5 References

[1] R.A. Sheldon, J.M. Woodley, Role of Biocatalysis in Sustainable Chemistry, Chem. Rev. 118 (2018) 801–838. https://doi.org/10.1021/acs.chemrev.7b00203.

[2] M. Markiton, S. Boncel, D. Janas, A. Chrobok, Highly active nanobiocatalyst from lipase noncovalently immobilized on multiwalled carbon nanotubes for Baeyer-Villiger synthesis of lactones, ACS Sustain. Chem. Eng. 5 (2017) 1685–1691. https://doi.org/10.1021/acssuschemeng.6b02433.

[3] Z. Qin, N. Feng, Y. Ma, Y. Li, L. Xu, Y. Wang, X. Fei, J. Tian, A lipase/poly (ionic liquid)-styrene microspheres/PVA composite hydrogel for esterification application, Enzyme Microb. Technol. 152 (2022) 109935. https://doi.org/10.1016/j.enzmictec.2021.109935.

[4] Y. Li, H. Wang, J. Lu, A. Chu, L. Zhang, Z. Ding, S. Xu, Z. Gu, G. Shi, Preparation of immobilized lipase by modified polyacrylonitrile hollow membrane using nitrile-click chemistry, Bioresour. Technol. 274 (2019) 9–17. https://doi.org/10.1016/j.biortech.2018.11.075.

[5] E.P. Cipolatti, N.S. Rios, J.S. Sousa, J. de M. Robert, A.A.T. da Silva, M.C.C. Pinto, A.B.C. Simas, E. Vilarrasa-García, R. Fernandez-Lafuente, L.R.B. Gonçalves, D.M.G. Freire, E.A. Manoel, Synthesis of lipase/silica biocatalysts through the immobilization of CALB on porous SBA-15 and their application on the resolution of pharmaceutical derivatives and on nutraceutical enrichment of natural oil, Mol. Catal. 505 (2021). https://doi.org/10.1016/j.mcat.2021.111529.

[6] M. Mathesh, B. Luan, T.O. Akanbi, J.K. Weber, J. Liu, C.J. Barrow, R. Zhou, W. Yang, Opening Lids: Modulation of Lipase Immobilization by Graphene Oxides, ACS Catal. 6 (2016) 4760–4768. https://doi.org/10.1021/acscatal.6b00942.

[7] J. Lu, Y. Li, H. Zhu, G. Shi, SiO2-Coated Fe3O4Nanoparticle/Polyacrylonitrile Beads for One-Step Lipase Immobilization, ACS Appl. Nano Mater. 4 (2021) 7856–7869. https://doi.org/10.1021/acsanm.1c01181.

[8] T.A. Costa-Silva, A.K.F. Carvalho, C.R.F. Souza, H.F. De Castro, L. Bachmann, S. Said, W.P. Oliveira, Enhancement lipase activity via immobilization onto chitosan beads used as seed particles during fluidized bed drying: Application in butyl butyrate production, Appl. Catal. A Gen. 622 (2021) 118217. https://doi.org/10.1016/j.apcata.2021.118217.

[9] S.P. De Souza, I.I. Junior, G.M.A. Silva, L.S.M. Miranda, M.F. Santiago, F. Leung-Yuk Lam,

A. Dawood, U.T. Bornscheuer, R.O.M.A. De Souza, Cellulose as an efficient matrix for lipase and transaminase immobilization, RSC Adv. 6 (2016) 6665–6671. https://doi.org/10.1039/c5ra24976g.

[10] S. Asmat, Q. Husain, M. Shoeb, M. Mobin, Tailoring a robust nanozyme formulation based on surfactant stabilized lipase immobilized onto newly fabricated magnetic silica anchored graphene nanocomposite: Aggrandized stability and application, Mater. Sci. Eng. C. 112 (2020) 110883. https://doi.org/10.1016/j.msec.2020.110883.

[11] J.M. Palomo, ChemComm, Chem. Commun. (2019). https://doi.org/10.1039/C9CC04944D.

[12] G. Kozma, A. Rónavári, Z. Kónya, Á. Kukovecz, Environmentally Benign Synthesis Methods of Zero-Valent Iron Nanoparticles, ACS Sustain. Chem. Eng. 4 (2016) 291–297. https://doi.org/10.1021/acssuschemeng.5b01185.

[13] R. Benavente, D. Lopez-Tejedor, J.M. Palomo, Synthesis of a superparamagnetic ultrathin FeCO3 nanorods-enzyme bionanohybrid as a novel heterogeneous catalyst, Chem. Commun. 54 (2018) 6256–6259. https://doi.org/10.1039/c8cc02851f.

[14] P. Nariya, M. Das, F. Shukla, S. Thakore, Synthesis of magnetic silver cyclodextrin nanocomposite as catalyst for reduction of nitro aromatics and organic dyes, J. Mol. Liq. 300 (2020) 112279. https://doi.org/10.1016/j.molliq.2019.112279.

[15] F. Shukla, T. Kikani, A. Khan, S. Thakore, α-Hydroxy acids modified β-cyclodextrin capped iron nanocatalyst for rapid reduction of nitroaromatics: A sonochemical approach, Int. J. Biol. Macromol. 209 (2022) 1504–1515. https://doi.org/10.1016/j.ijbiomac.2022.04.149.

[16] N. Bensabeh, A. Moreno, A. Roig, M. Rahimzadeh, K. Rahimi, J.C. Ronda, V. Cádiz, M. Galià, V. Percec, C. Rodriguez-Emmenegger, G. Lligadas, Photoinduced Upgrading of Lactic Acid-Based Solvents to Block Copolymer Surfactants, ACS Sustain. Chem. Eng. 8 (2020) 1276–1284. https://doi.org/10.1021/acssuschemeng.9b06599.

[17] L.R. Lawin, W.K. Fife, C.X. Tian, Hydrolysis of p-nitrophenyl esters in the presence of polymer micelles. Selectivity and biphasic behavior with increasing ester concentration, Langmuir. 16 (2000) 3583–3587. https://doi.org/10.1021/la980486l.

[18] H. Li, L. Ma, L. Zhou, J. Gao, Z. Huang, Y. He, Y. Jiang, An integrated nanocatalyst combining enzymatic and metal-organic framework catalysts for cascade degradation of organophosphate nerve agents, Chem. Commun. 54 (2018) 10754–10757.

https://doi.org/10.1039/C8CC06727A.

[19] K. Iqbal, A. Iqbal, A.M. Kirillov, C. Shan, W. Liu, Y. Tang, A new multicomponent CDs/Ag@Mg-Al-Ce-LDH nanocatalyst for highly efficient degradation of organic water pollutants, J. Mater. Chem. A. 6 (2018) 4515–4524. https://doi.org/10.1039/c8ta00258d.

[20] R. Tao, M. Gao, F. Liu, X. Guo, A. Fan, D. Ding, D. Kong, Z. Wang, Y. Zhao, Alleviating the Liver Toxicity of Chemotherapy via pH-Responsive Hepatoprotective Prodrug Micelles, ACS Appl. Mater. Interfaces. 10 (2018) 21836–21846. https://doi.org/10.1021/acsami.8b04192.

[21] S. Imai, M. Takenaka, M. Sawamoto, T. Terashima, Self-Sorting of Amphiphilic Copolymers for Self-Assembled Materials in Water: Polymers Can Recognize Themselves, J. Am. Chem. Soc. 141 (2019) 511–519. https://doi.org/10.1021/jacs.8b11364.

[22] N.U. Deshpande, M. Jayakannan, Cisplatin-Stitched Polysaccharide Vesicles for Synergistic Cancer Therapy of Triple Antagonistic Drugs, Biomacromolecules. 18 (2017) 113–126. https://doi.org/10.1021/acs.biomac.6b01411.

[23] R. Aluri, S. Saxena, D.C. Joshi, M. Jayakannan, Multistimuli-Responsive Amphiphilic Poly(ester-urethane) Nanoassemblies Based on 1 -Tyrosine for Intracellular Drug Delivery to Cancer Cells, Biomacromolecules. 19 (2018) 2166–2181. https://doi.org/10.1021/acs.biomac.8b00334.

[24] Z. Zhang, X. Chen, X. Gao, X. Yao, L. Chen, C. He, X. Chen, Targeted dextran-b-poly(ε-caprolactone) micelles for cancer treatments, RSC Adv. 5 (2015) 18593–18600. https://doi.org/10.1039/c4ra15696j.

[25] Y. Zhong, W. Yang, H. Sun, R. Cheng, F. Meng, C. Deng, Z. Zhong, Ligand-directed reduction-sensitive shell-sheddable biodegradable micelles actively deliver doxorubicin into the nuclei of target cancer cells, Biomacromolecules. 14 (2013) 3723–3730. https://doi.org/10.1021/bm401098w.

[26] D. Šmejkalová, K. Nešporová, G. Huerta-Angeles, J. Syrovátka, D. Jirák, A. Gálisová, V. Velebný, Selective in vitro anticancer effect of superparamagnetic iron oxide nanoparticles loaded in hyaluronan polymeric micelles, Biomacromolecules. 15 (2014) 4012–4020. https://doi.org/10.1021/bm501065q.

[27] S. Zhu, S.H. Ho, X. Huang, D. Wang, F. Yang, L. Wang, C. Wang, X. Cao, F. Ma, Magnetic

Nanoscale Zerovalent Iron Assisted Biochar: Interfacial Chemical Behaviors and Heavy Metals Remediation Performance, ACS Sustain. Chem. Eng. 5 (2017) 9673–9682. https://doi.org/10.1021/acssuschemeng.7b00542.

[28] B.H. San, S. Ravichandran, K.S. Park, V.K. Subramani, K.K. Kim, Bioinorganic Nanohybrid Catalyst for Multistep Synthesis of Acetaminophen, an Analgesic, ACS Appl. Mater. Interfaces. 8 (2016) 30058–30065. https://doi.org/10.1021/acsami.6b12875.

[29] D. Mandal, M. Ghosh, S. Maiti, K. Das, P.K. Das, Water-in-oil microemulsion doped with gold nanoparticle decorated single walled carbon nanotube: Scaffold for enhancing lipase activity, Colloids Surfaces B Biointerfaces. 113 (2014) 442–449. https://doi.org/10.1016/j.colsurfb.2013.09.047.

[30] M. Cortes-Clerget, N. Akporji, J. Zhou, F. Gao, P. Guo, M. Parmentier, F. Gallou, J.Y. Berthon, B.H. Lipshutz, Bridging the gap between transition metal- and bio-catalysis via aqueous micellar catalysis, Nat. Commun. 10 (2019) 1–10. https://doi.org/10.1038/s41467-019-09751-4.

[31] R. Joncour, N. Duguet, E. Métay, A. Ferreira, M. Lemaire, Amidation of phenol derivatives: A direct synthesis of paracetamol (acetaminophen) from hydroquinone, Green Chem. 16 (2014) 2997–3002. https://doi.org/10.1039/c4gc00166d.

[32] P. Gopinathan, S., Gopinathan, C., Kuruvilla, J., Pardhy, S. A., Ratnasamy, Process for the preparation of N-acetyl aminophenols, United States Pat. (1999) 3–6.

[33] I. Sádaba, M.L. Granados, A. Riisagerc, E. Taarninga, Deactivation of solid catalysts in liquid media: The case of leaching of active sites in biomass conversion reactions, Green Chem. 17 (2015) 4133–4145. https://doi.org/10.1039/b000000x.
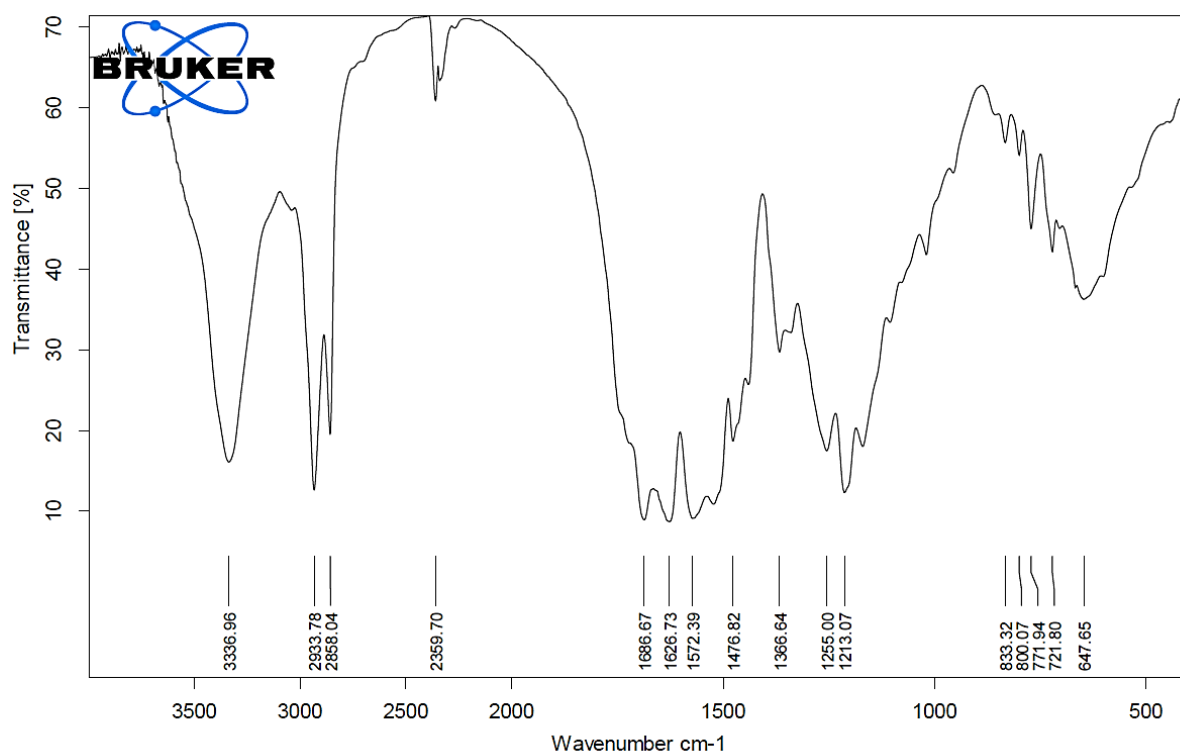
Spectral data
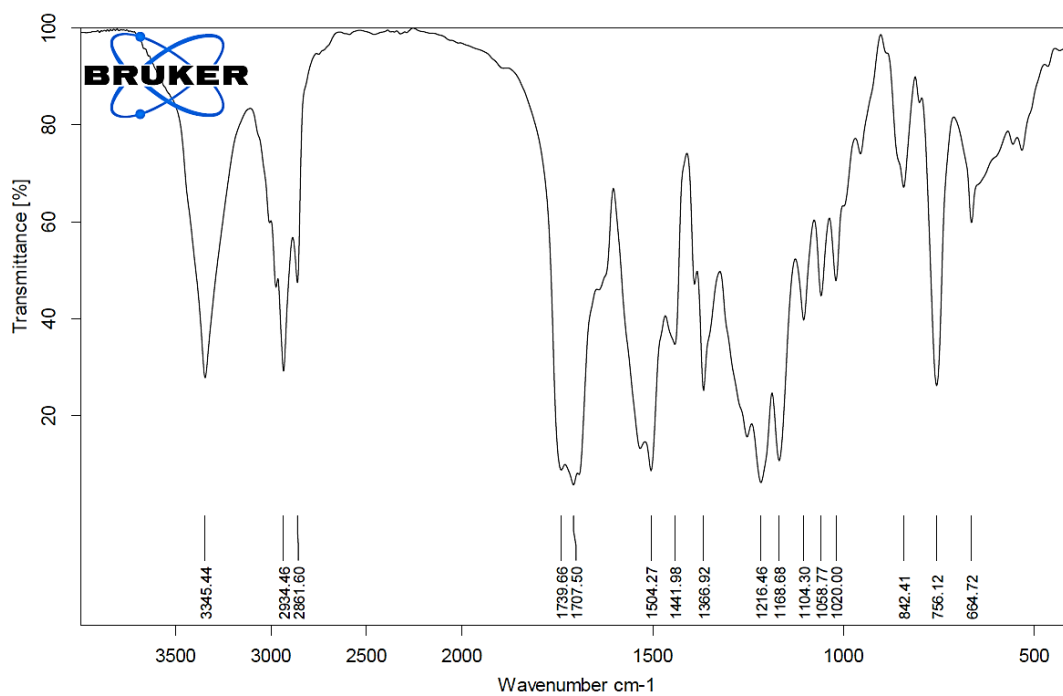
Figure S1: FTIR spectrum of Pre-polymer 1

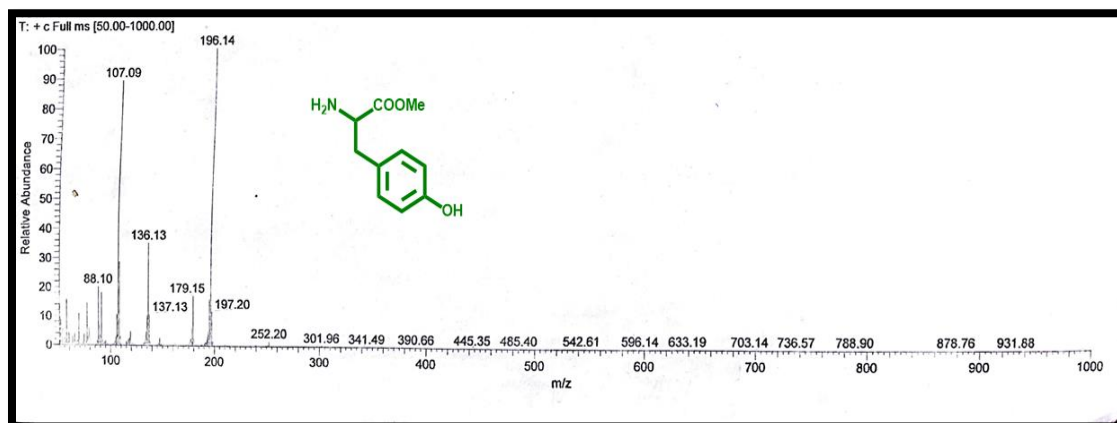**Figure S2: FTIR spectrum of Pre-polymer 2**

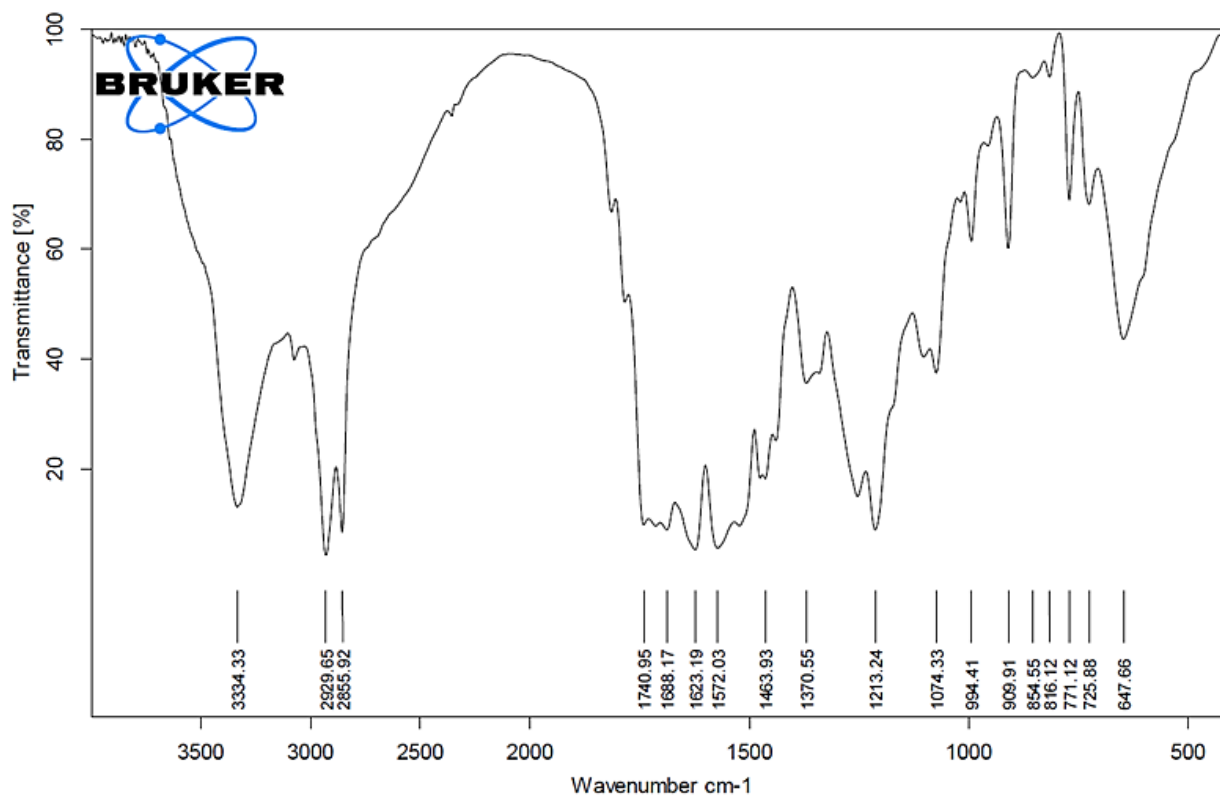**Figure S3: Mass spectrum of L-Tyrosine methyl ester**
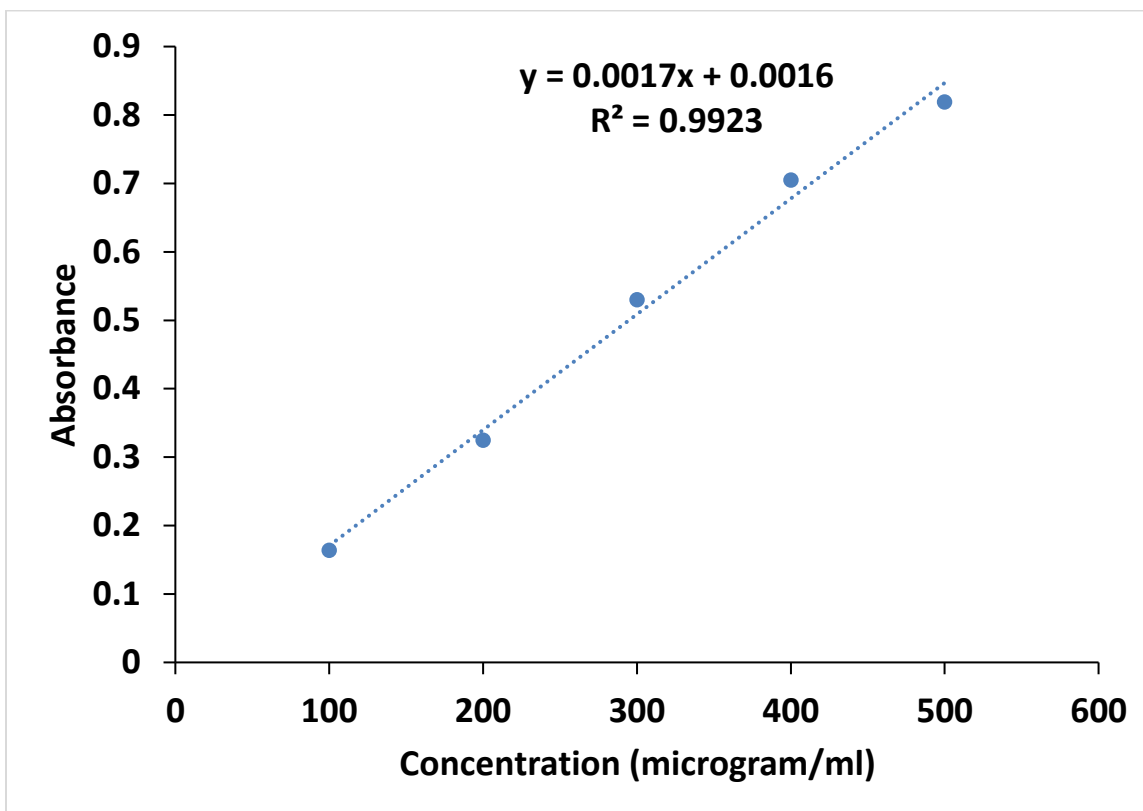

Figure S4: FTIR spectrum of Pre-polymer 3
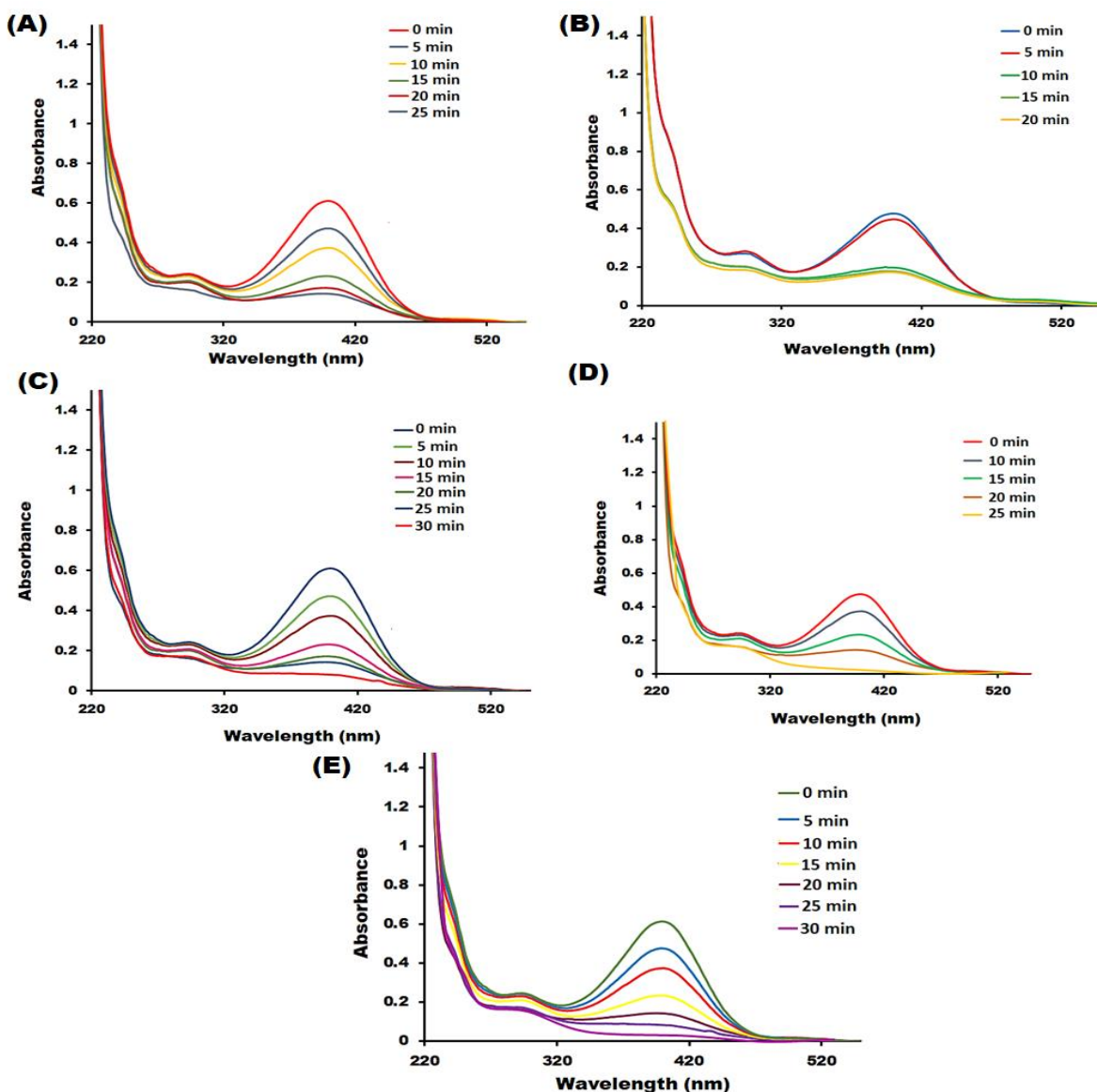
Figure S5: Caliberation plot of BSA

Figure S6: The time dependent UV–vis absorption spectra of 4-NP reduction (hydrogenation step) and the dependence of ln(C/Co) versus time plot for the pseudo-first-order reaction kinetics in the presence of nZVI-CALB@NM at 35 ◦C. UV-visible spectra of (A) p-nitrophenyl butyrate, (B) p-nitrophenyl chloroformate (C) p-nitrophenyl decanoate, (D) p-nitrophenyl octanoate and (E) p-nitrophenyl palmitate.